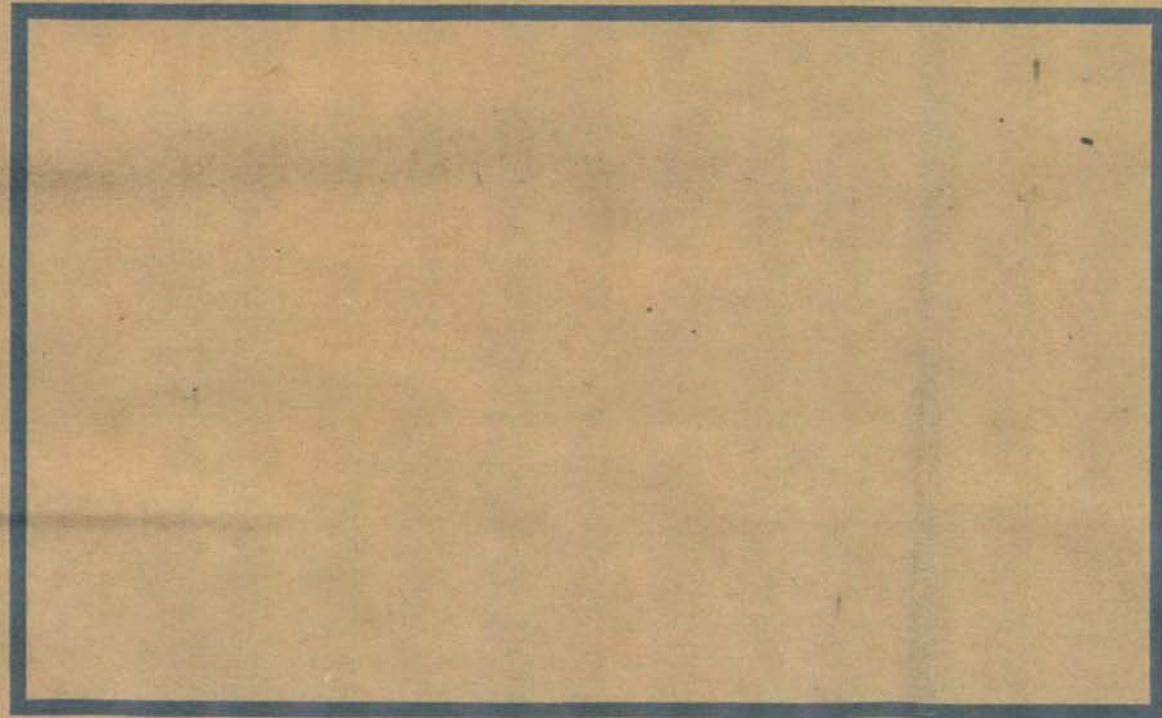


ENG 279-(EQC 1999/345)

**Estimation of Soil Shear Modulus Softening during Strong
Ground Shaking using Ground Surface and Downhole
Acceleration Recordings**

R O Davis, J B Berrill, Soils & Seismology



Estimation of soil shear modulus softening during strong ground shaking using ground surface and downhole acceleration recordings

R. O. Davis*

Department of Civil Engineering, University of Canterbury, Christchurch, New Zealand

SUMMARY

An algorithm for estimating the average shear modulus for a soil site containing a downhole accelerometer array is described. For distant or weak earthquakes, the usual procedure for estimating shear modulus is to perform time-series correlation of two downhole records. The vertical distance between instruments divided by the peak correlation lag time gives the average shear wave velocity. The shear modulus follows easily. This method is not applicable for stronger earthquakes where non-linear softening effects lead to progressively slower shear wave velocities. The method presented here overcomes the softening effect by compressing the time scale of the upper acceleration record. Time compression is accomplished in such a way that the peak correlation of the two records is maximized. The algorithm steps through the records, maximizing the correlation peak by adjusting the time scale within an active time interval. The resulting compressed upper record can be interpreted as the ground motion that would have occurred had softening not taken place. The summation of the various time scale adjustments shows both the amount of softening and the time at which it occurred. Copyright © 2000 John Wiley & Sons, Ltd.

KEY WORDS: downhole arrays; shear modulus; shear wave velocity; softening; cross-correlation

INTRODUCTION

Vertical arrays of accelerometers spaced at intervals of 10–20 m have been placed at a number of sites throughout the world [1–4]. They are generally referred to as downhole arrays. Their central purpose is to provide direct measurement of site amplification effects. The resulting acceleration records from different depths provide valuable insight into the propagation and modification of seismic waves in the site soils. Interpretation of data from a recorded event is relatively

* Correspondence to: R. O. Davis, Department of Civil Engineering, University of Canterbury, Private Bag 4800, Christchurch, New Zealand

Contract/grant sponsor: New Zealand Earthquake Commission Research Foundation; contract/grant number: 99/345

Received 23 July 1998

Revised 29 June 1999

Accepted 24 August 1999

straightforward for small or distant earthquakes where the ground deformation is relatively small and elastic behaviour predominates. In these cases investigators normally model the soil response using vertically propagating SH waves. There is a requirement of course for shear moduli values in order to specify shear wave velocities. Estimates of shear modulus for the soils involved may be obtained by several means including laboratory tests, field seismic profiling, or time-series correlation of the downhole records themselves.

Shear moduli are not so easily estimated for stronger earthquakes when softening due to non-linear soil behaviour may introduce unwanted complications. In stronger events the site soils may undergo progressive changes depending on the levels of stress and strain and (for saturated soils) pore pressure increase. It is not nearly so easy to estimate shear moduli for these circumstances. Clearly field seismic profiling is inappropriate as only small strain deformations are involved. Laboratory tests can be adapted to simulate the estimated stress history, but there are obvious difficulties in synthesizing an appropriate stress history and then implementing it in the lab.

Often, time-series correlation of downhole acceleration records from two depths has been used to estimate the average velocity of waves propagating between those depths. The time-series correlation directly provides an estimate for the lag or travel time for waves to propagate from the lower depth to the higher. The wave velocity is obtained by dividing the distance between instruments by the peak correlation lag time. Wave velocities can then be easily translated into modulus values. This method is clearly appropriate, provided the level of ground motion is not sufficiently strong to result in significant non-linear soil behaviour. As an example, Elgamal *et al.* [4] used time-series correlation for a variety of small earthquakes to assess the shear wave velocity structure at the SMART1 Lotung downhole test site in Taiwan. The data developed in [4] were later used in the analysis of stronger motion data from larger earthquakes at the test site [5].

Problems arise with correlation of records when stronger levels of shaking occur. In those cases, early parts of the acceleration history will correspond to the generally stiffer small deformation moduli values that initially exist at the site. As shaking progresses the moduli may soften and the wave travel time between the instrument locations in the downhole array will lengthen. This lengthening may be significant whenever the shaking is sufficiently strong to generate non-linear effects. If one now correlates the two entire records, the calculated lag will reflect neither the initial small deformation behaviour nor the later softened behaviour. Instead one obtains an average lag lying somewhere between the initial and softened values. Several investigators have used a variety of methods to overcome this difficulty. Resonant frequencies determined from Fourier spectral ratios were used by Chang *et al.* [6] to estimate shear wave velocities at the Lotung SMART 1 array. A similar analysis was carried out by Wen *et al.* [7]. In a separate efforts, Li *et al.* [8] employed a sophisticated hypoplasticity model to numerically simulate ground motion at the Lotung site, while Kazama [9] directly approximated shear stress and strain for the Kobe Port Island downhole acceleration records. None of these methods enjoy the simplicity and directness associated with simple correlation of two downhole records.

This paper attempts to overcome the problem described above. Consider the typical two-instrument downhole array sketched in Figure 1. It is desired to obtain a continuous history of shear wave velocity (or the corresponding shear modulus) throughout the times where shaking and softening occur. We will present a technique for compressing the time scale of the upper acceleration time history in such a way as to precisely counteract the effects of softening. The new, compressed acceleration history will represent the soil response without softening effects. Its

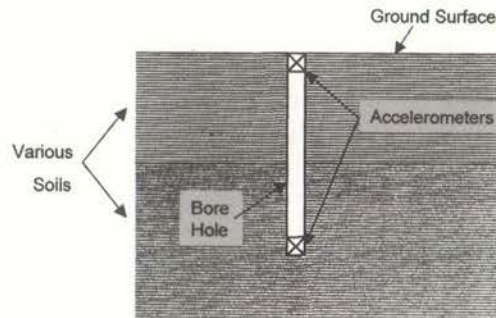


Figure 1. Typical downhole accelerometer array.

correlation with the buried instrument record will approximate the small deformation response of the intervening soils just as would be the case if no softening had occurred. Meanwhile, the amount of time compression suffered by the upper record will tell us how much softening has occurred and when it occurred. It will be possible to construct a complete picture of the average shear wave velocity between the two instrument levels throughout the duration of the earthquake.

There are several possible applications for the softened shear modulus history. One can directly compare field softening data with published models for shear modulus reduction such as given by Seed *et al.* [10]. In instances where liquefaction has been observed, the softening history may give considerable insight into both the onset of liquefaction and the later solidification process. Comparison and verification of analytical site amplification models are possible as well.

The algorithm developed below is quite robust. It provides as much detail as the user requires, consistent with the time scale for the acceleration records and the distance between the downhole instruments. The method will be illustrated by considering a case history in which extreme amounts of softening occurred: the downhole acceleration records from the Port Island array at Kobe.

BACKGROUND

The basic elements of our method are most easily described by reference to specific downhole records. Therefore, we begin by considering the Kobe Port Island East–West accelerations from the 0 and 16 m depths illustrated in Figure 2. The aim of our analysis is to estimate the average shear modulus, or equivalently the shear wave velocity, in the upper 16 m, *continuously* throughout the earthquake. Liquefaction was observed at this site and it is clear significant softening occurred during the earthquake.

The full 60 s of shaking shown in Figure 2 is difficult to consider in detail because of the small time scale necessitated by the size of the figure. A more informative picture is developed if we expand the time scale. This has been done in Figure 3 where the time interval between 12 and 20 s has been isolated. It is clear from this figure that marked correlation exists between the two records. The wave crests denoted A, B and C strongly suggest upward propagating shear waves that, with only minor changes of wave form, move from the 16 m depth to the soil surface.

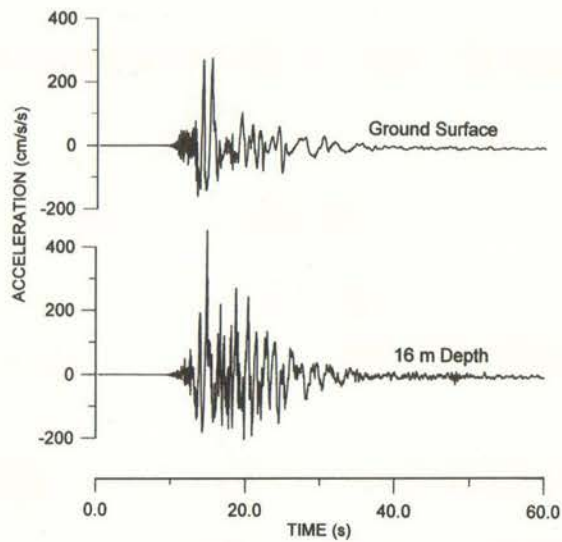


Figure 2. Kobe Port Island acceleration records. East-West data from 0 and 16 m depths.

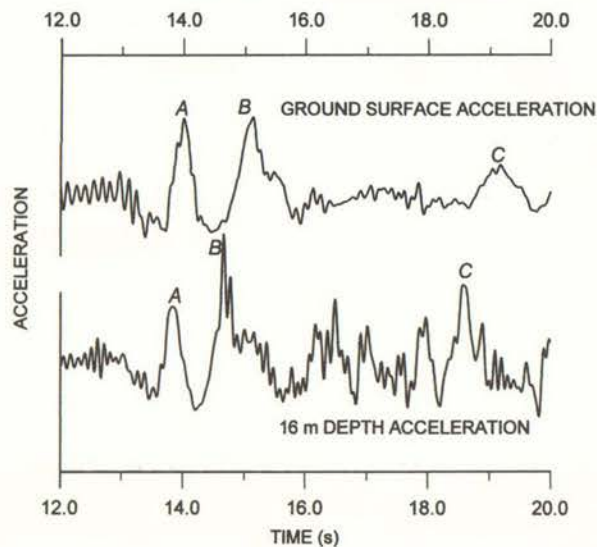


Figure 3. Expanded segment of data from Figure 2.

However, closer inspection shows that the lag times associated with the three wave crests are significantly different. Examining the digitised records, we find the lag for peak A is 0.17 s, for peak B it is 0.46 s, and for peak C, 0.61 s. The increasing time lag results from the extreme softening of the site during the time interval shown in Figure 3.

We can attempt to better understand the Kobe response by examining the correlation of the two records. The discrete-time series correlation of two sampled functions $a_k = a(t_k)$ and $b_k = b(t_k)$ is defined as [11]

$$\Gamma(t_m) = \sum_k b_{k+m} a_k \quad (1)$$

where the sum is taken over the entire record. Often Γ is given in normalised form,

$$\Gamma_n(t_m) = \frac{\Gamma(t_m)}{(\sum_k a_k^2)^{1/2} (\sum_k b_k^2)^{1/2}} \quad (2)$$

Direct calculation of Γ using Equation (1) can be seriously time consuming for long records. In practice, one uses the discrete correlation theorem which states that Γ is one member of the discrete Fourier transform pair

$$\Gamma(t_k) \Leftrightarrow B_k A_k^* \quad (3)$$

Here A_k and B_k are the discrete Fourier transforms of a_k and b_k and $*$ denotes complex conjugation. A_k and B_k are found using fast Fourier transforms of the given data. The inverse FFT is then used to find Γ . The resulting calculation is extremely efficient.

The functions Γ and Γ_n will both show a peak at the value of t_k corresponding to the lag or time delay between the two records. The normalized correlation for the two Kobe records is shown in Figure 4. We see a strong peak at $t = 0.31$ s. This is the calculated lag for the two records. The corresponding shear wave velocity is $16 \text{ m}/0.31 \text{ s} = 51.6 \text{ m/s}$. This value is, at best, an average wave velocity for the entire time interval of the record. It cannot represent the softening behaviour of the site soils as shaking progresses.

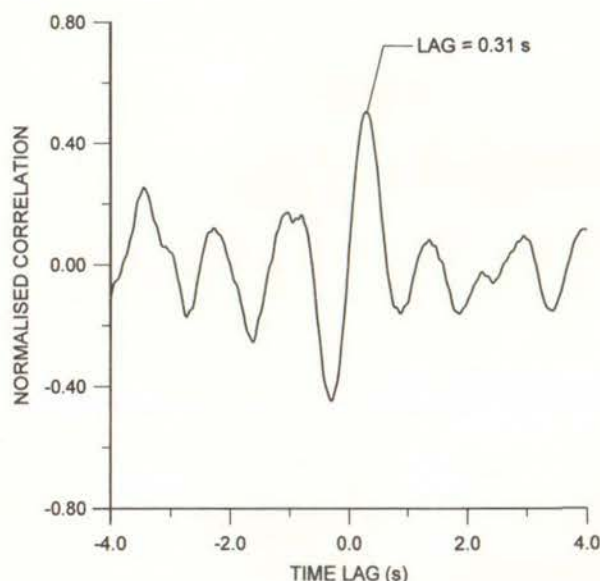


Figure 4. Normalized correlation of East-West Port Island records.

One approach to dealing with softened records such as Kobe is to break down the two records into distinct windows and consider the individual correlations for each window. This was done for the Kobe records by Elgamal *et al.* [12]. Their results indicate a dramatic reduction in soil stiffness, but lack fine detail regarding the continuous variation of shear wave velocity or shear modulus. The basic problem with this method lies in the size of the record segments to be used. The segments must be sufficiently large to be representative of some part of the record. The resulting lag is a single number associated in some (not fully specified) way with the segment. If the segment is made too small, the desired correlation will often be lost and spurious values for the lag may result. We will compare this method with the proposed algorithm later in the paper.

ANALYSIS

Our aim here is to use the correlation of two records as a tool to lead to a continuous picture of the shear wave velocity. The idea is to maximize the correlation by non-linearly compressing the time scale of the upper acceleration record. Referring again to Figure 3, it is clear that compressing the time scale of the upper record in some appropriate way could lead to better correlation of the two records. If the correct amount of time compression were put in place, the increasing lag associated with wave crests B and C could be completely eliminated and all three peaks could have the same lag. The effect on the correlation function Γ shown in Figure 4 would be twofold: first the peak at 0.31 s would be shifted to the left, second the magnitude of the correlation peak would be increased. This suggests that we could use the magnitude of the peak value of Γ as a criterion for adjusting the time scale of the upper record.

Next, we realize that if the time scale is compressed, the amount of compression necessary to maximize the correlation will be equal to the amount by which softening of the site soil has lengthened the travel time between the two instruments. If we divide the distance between the instruments by the sum of the travel time for small deformation elastic waves plus the amount of time compression, the result should be the shear wave velocity corresponding to the softened soil profile. This is the basic idea of our analysis.

In more detail, we proceed as follows. Suppose we have two sampled acceleration records denoted a_k and b_k such as those shown in Figure 2. Let a_k be the record from the higher instrument. Also, let the time corresponding to a_k and b_k be t_k , and assume the time increment δt between samples is a constant. Now, consider a new time scale denoted \hat{t}_k where time is compressed in some segment of the record. We define \hat{t}_k as follows:

$$\hat{t}_k = \begin{cases} t_k & \text{for } t_k \leq t_S \\ t_k - \Delta \left(\frac{t_k - t_S}{t_F - t_S} \right) & \text{for } t_S < t_k \leq t_F \\ t_k - \Delta & \text{for } t_F < t_k \end{cases} \quad (4)$$

Here \hat{t}_k is the compressed time, t_S and t_F are the start and finish times for the compressed segment, and Δ is the total amount of compression at the end of the segment. Time is compressed linearly between t_S and t_F and we continue throughout the remainder of the record using a constant time translation Δ . An example of a compressed time scale is shown schematically in Figure 5. In the figure the compression Δ has been taken as 0.50 s and the values of t_S and t_F are 14.0 and 16.0 s. The new compressed time is shown by the solid line while the dashed 45° line is simply a plot of

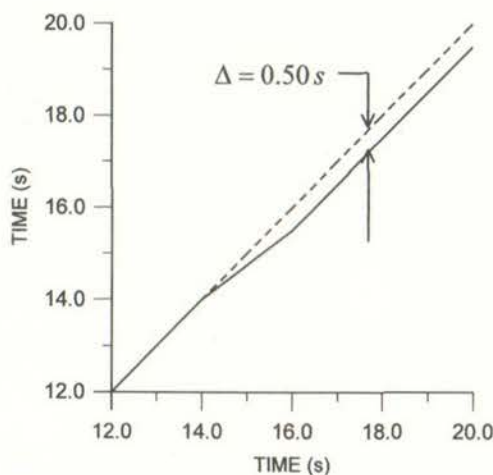


Figure 5. Example of compressed time scale.

the original time versus itself. Note that the new compressed time \hat{t}_k will no longer have a constant increment size δt on the interval $[t_s, t_F]$ and the values of \hat{t}_k and t_k will generally be different for all times greater than t_s .

Next, we rewrite the upper acceleration record, interpolating the values of acceleration at the appropriate times in the newly compressed time scale. In this way, we realign the new compressed acceleration record with the original sampling times. This is necessary in order that we can carry out the correlation of the new record with the original b_k acceleration record. We rewrite the record as follows. For any desired value of time t_j in the original time base, we find the corresponding acceleration using linear interpolation

$$\hat{a}_j = a_k + (a_{k+1} - a_k) \left(\frac{t_j - \hat{t}_k}{\hat{t}_{k+1} - \hat{t}_k} \right) \quad (5)$$

Here \hat{a}_j is the new interpolated acceleration at time t_j , \hat{t}_k is compressed time, a_k is the acceleration corresponding to \hat{t}_k . The index k is selected so that $\hat{t}_k \leq t_j \leq \hat{t}_{k+1}$. It is a simple matter to sweep through the compressed record interpolating the new acceleration values. The results of this effort are new accelerations based on the compressed time scale, but now properly aligned with the original time base. An example is illustrated in Figure 6. The time interval for compression is defined by $t_s = 14.0$ s and $t_F = 16.0$ s. For purposes of illustration, the value of Δ has been set equal to 0.25 s. In practice, the value of Δ will be determined by maximising the correlation. Also, the interval to be compressed will generally be considerably shorter than 2 s, but a large value is useful to illustrate the concepts involved. In Figure 6 the dashed line is the original acceleration record and the solid line the compressed record. Note how the compression is initiated at $t_s = 14.0$ s and how the amount of compression remains constant for times greater than $t_F = 16.0$ s.

Our algorithm for estimating shear wave velocity is outlined in Figure 7. We begin by partitioning the time scale for the complete record into M segments $(t_F - t_s)$ of equal size. Then beginning with segment one, we maximize the peak value of the correlation Γ by adjusting the

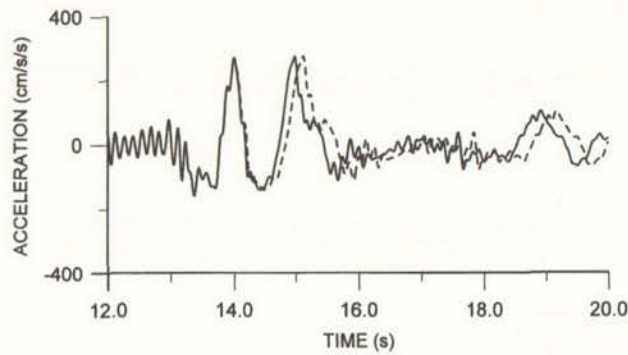


Figure 6. Example of effect of compressed time on ground surface acceleration from Port Island.

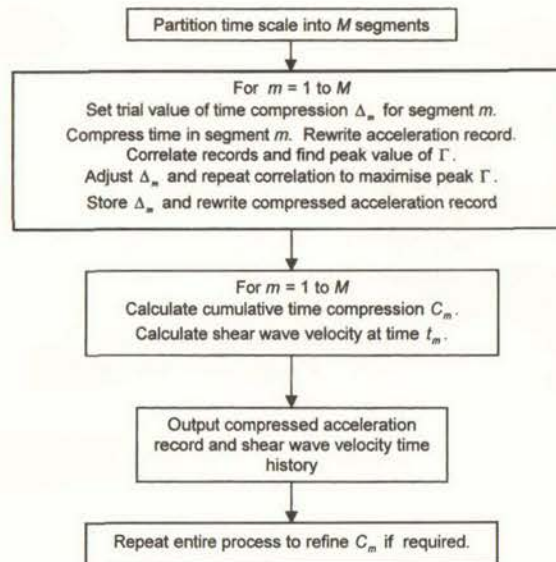


Figure 7. Flow diagram for time compression algorithm.

value of the compression Δ_1 . Note that the correlation is made using the entire record. The compression of segment one not only affects the record within the segment but also at all later times. We then move forward to segment 2, maximizing Γ to find Δ_2 , and so on through the record, stopping only when the shaking becomes too weak to be of interest or when the values of Δ_m become very small in comparison to the segment size. Next, we note the Δ_m 's for each segment have a cumulative effect on all the record that follows. Therefore, we construct the cumulative time compression C_m according to

$$C_m = \sum_{i=1}^m \Delta_i \quad m = 1, 2, \dots, M \quad (6)$$

The value of C_m represents the time compression required to offset the softening effect caused by strong shaking in the soil up to the time corresponding to the end of segment m .

Once time compression is complete, the two acceleration records will be correlated with a lag time corresponding to the initial small deformation shear modulus of the soil before softening commenced. This lag can be read off the final correlation. Let its value be t_0 . We can now construct the shear wave velocity history as

$$v_s(t_m) = \frac{\text{distance between instruments}}{t_0 + C_m} \quad (7)$$

Here t_m denotes the time at the end of segment m .

In the next section we will show a typical application using the Kobe Port Island records. However, before doing this, three points should be noted. The first concerns the problem of optimizing the magnitude of the correlation peak by adjusting the value of the time compression Δ_m for segment m . This is a relatively simple one-dimensional optimization problem. Several different optimizing schemes were tried while the algorithm was under development. The most effective, from the standpoint of being both straightforward and highly stable, was the golden section algorithm. The subroutines GOLDEN and MBRAK from *Numerical Recipes in Fortran* [13] were employed directly. The MBRAK routine first brackets the optimal compression value. Then GOLDEN refines the value to within the desired tolerance. For the Kobe analysis described below, the tolerance was set equal to 0.01 s, the value of the time interval for the acceleration records.

The second point to note here is that the entire algorithm outlined above may be repeated. That is, the fully compressed record emerging at the conclusion of the optimization may be reused as if nothing had occurred. The result is a new cumulative time compression, say C'_m . We may then sum C_m and C'_m to obtain a refined time compression. Experience suggests the best procedure is to first run the algorithm with a relatively large time interval ($t_F - t_S$) and then to repeat the process with the time interval halved. A third calculation, with ($t_F - t_S$) halved again, may be performed and so on. At each stage more detail is added to the time compression record.

Our third comment follows from the second. The magnitude of ($t_F - t_S$) is of considerable significance to the overall result. If we attempt to make the interval ($t_F - t_S$) too small, we risk overemphasizing the importance of a small segment of the record. For the Kobe records considered below, we used an initial interval ($t_F - t_S$) of 0.8 s. Halving this to 0.4 s leads to improvement in the degree of detail embodied in the results. Halving again to 0.2 s yields more detail but does not appear to cause significant improvement. A fourth attempt at 0.1 s generates slightly more detail but is of questionable value. It is important to keep in mind that, at best, we can hope for no more than an accurate representation of the *average* shear wave velocity between the depths of the instruments involved. Other effects such as soil layering, P-waves and surface waves have undoubtedly contaminated the records to some extent and use of an excessively small interval ($t_F - t_S$) may unduly emphasize their importance.

A second problem can also arise when too small an interval ($t_F - t_S$) is used. As in almost any optimization problem, our objective function (the peak correlation value) has multiple extrema. This is sometimes referred to as the bumpy mattress problem. We seek to smoothly follow one extreme value as the algorithm sweeps through the record, but it is always possible to jump to another nearby peak that may temporarily appear more attractive to the program. It is not difficult to identify this phenomenon since, if it occurs, the lag time will undergo a sudden

dramatic change. We can generally avoid the problem by using larger intervals ($t_F - t_S$) since they will generally encompass sufficient wave complexity to preclude an easy path for the optimization to take to a spurious peak. On the other hand, small intervals may invite a jump to a nearby local extremum. For this reason, as well as the comment above, small time intervals are not recommended.

EXAMPLE: KOBE PORT ISLAND

Consider once again the East–West acceleration records from the ground surface and 16 m depth at Port Island shown in Figures 2 and 3. We have carried out the programme of calculations outlined above using a time interval of 0.8 s. Figure 8 shows the normalized correlation functions Γ_n for the records both before and after time compression. The dashed line in Figure 8 is identical to the correlation shown in Figure 4. The solid line shows the correlation after time compression. From Figure 8, we see that the magnitude of the peak correlation has been significantly improved (from 0.504 to 0.651) by the compression. We also see the lag has been reduced to 0.07 s. This value suggests an initial small deformation shear wave velocity of $16 \text{ m}/0.07 \text{ s} = 228 \text{ m/s}$. Figure 9(a) shows the cumulative time compression C_m plotted versus time. The calculation begins at $t = 5 \text{ s}$, and for a little more than 7 s C_m remains equal to zero. No time compression occurs in this early part of the record. Around 12 s there is a slight *stretching* of the time scale, indicated by the small negative jump in C_m . Then between 13 and 14 s a rapid compression is found. This part of the record evidently contains the most marked softening of the site soils. A second episode of softening is evident at 25 s, but this is followed by a decrease in C_m indicating stretching of the time scale is required by the algorithm. The computation was stopped at 50 s.

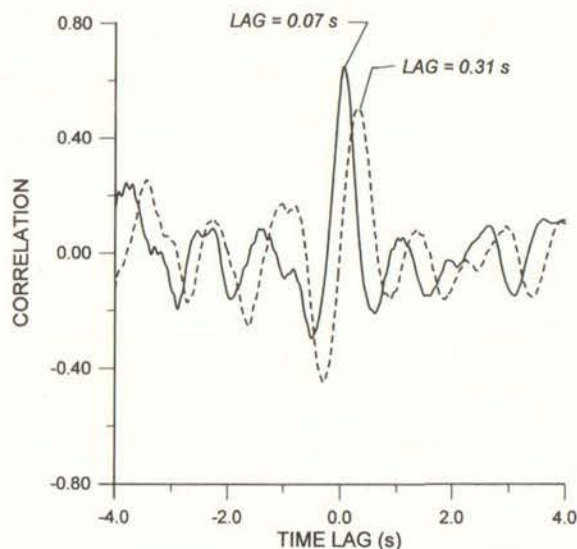


Figure 8. Correlation of Port Island East–West data from 0 and 16 m: dashed line shows correlation of original data; solid line shows correlation after time compression.

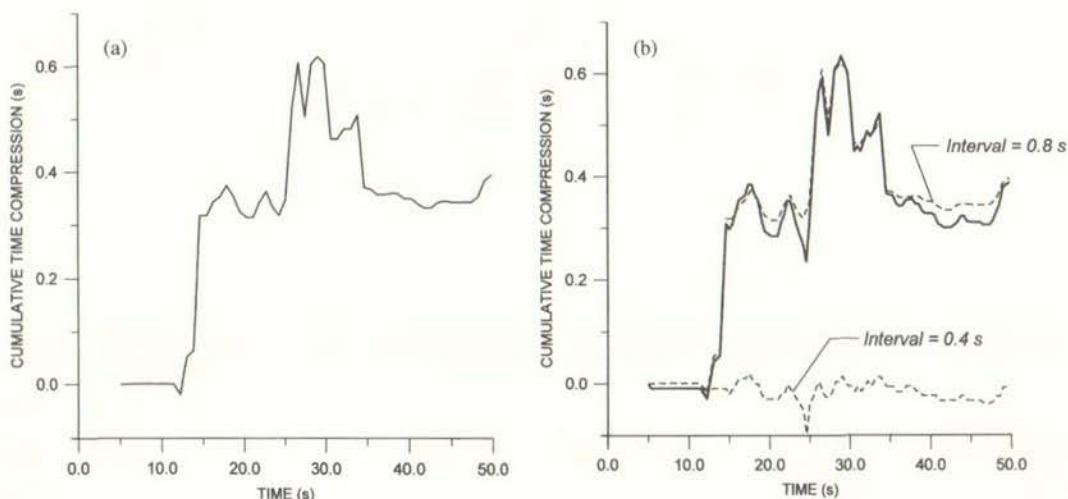


Figure 9. Cumulative time compression for surface acceleration record for Port Island East-West record. (a) Results for 0.8 s intervals. (b) Results after halving the time interval.

Figure 9(b) illustrates the second compression of the record, now using an interval ($t_F - t_S$) of 0.4 s. The compressed upper record from the previous calculation is used as input for this calculation. As one might expect, the resulting time compression is generally small. It is shown by the dashed line hovering around zero compression near the bottom of the figure. The original, 0.8 s interval, cumulative compression is also shown by the second dashed line. The summation of the two lines is shown as the solid line. It seems evident from the figure that additional detail has been added to the original result, but the overall trend in the compression is largely preserved. The magnitude of the peak correlation is increased by this second calculation to a value of 0.692. The lag time remained steady at 0.07 s.

Figure 10 shows the segment of the ground surface acceleration history between 12 and 20 s. The dashed line represents the original acceleration history while the solid line shows the compressed history after the above calculations. Significant amounts of time compression are evident near 14 s. In Figure 11 we have replotted both the upper (compressed) and lower acceleration records, and we have offset the two records by the final lag of 0.07 s. In comparison with Figure 3, it can be seen from this figure how the two records are now visually well correlated.

As we noted above, it is possible to continue repeating the calculation with progressively smaller time increments. Figure 12 illustrates the result of this process for intervals of 0.2 and 0.1 s. The heavy solid line represents the situation following the 0.4 s interval compression. That line is the same as the solid line in Figure 9(b). The dashed line shows the result from the 0.2 s compression and the light solid line shows the 0.1 s calculation. Inspecting the figure we see the smaller time intervals tend to exaggerate some of the peaks in the earlier result. The degree of exaggeration is not large, yet one must doubt their validity for the reasons discussed above. The peak correlation is not greatly increased by either of the new calculations. Its value increases to 0.704 for the 0.2 s run, and to 0.706 for the 0.1 s calculation. The lag time remained steady at 0.7 s throughout both calculations.

As mentioned above, another approach to our problem is individually correlating the two records over individual time windows. Figure 13(a) shows results from such a computation. The

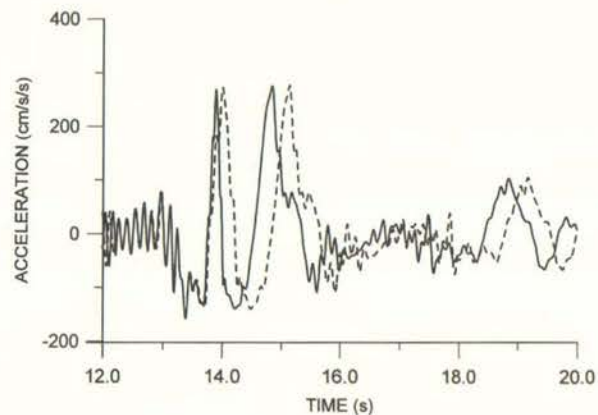


Figure 10. Part of the ground surface acceleration record before and after time compression.

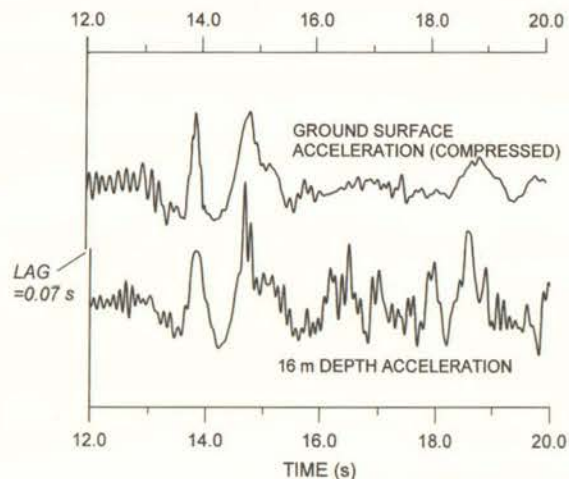


Figure 11. Comparison of 0 and 16 m East-West records after time compression of upper record. Here the 16 m record is offset by 0.07 s.

diamond-shaped data points on the figure represent lag times associated with correlations for a window of 6.4 s duration moving across the entire record. Each of the data points results from correlating the two acceleration records over the time window and then plotting the lag versus the time at the centre of the window. If one halves the window size to 3.2 s, the results become erratic and many points plot well off the scale of the graph. In order to compare these results with the time compression method, we have biased the data in the figure downward by 0.7 s. This accounts for the time compression results being the *additional* lag time over and above the lag associated with small deformation elastic waves. The time compression result for the interval ($t_F - t_S$) of 0.4 s is shown by the dashed line on the figure. There are similarities between the two data sets but there are significant differences in the timing of the major softening jumps. We can easily discover

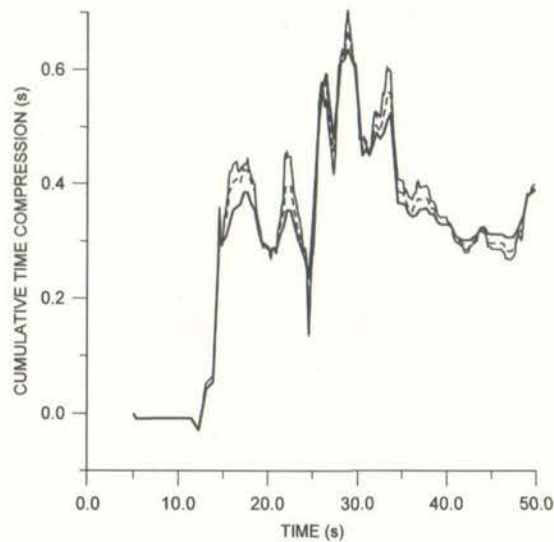


Figure 12. Effect of further halving time interval on cumulative time compression. Heavy solid line is identical to that in Figure 9. Dashed line corresponds to 0.2 s intervals, light solid line to 0.1 s intervals.

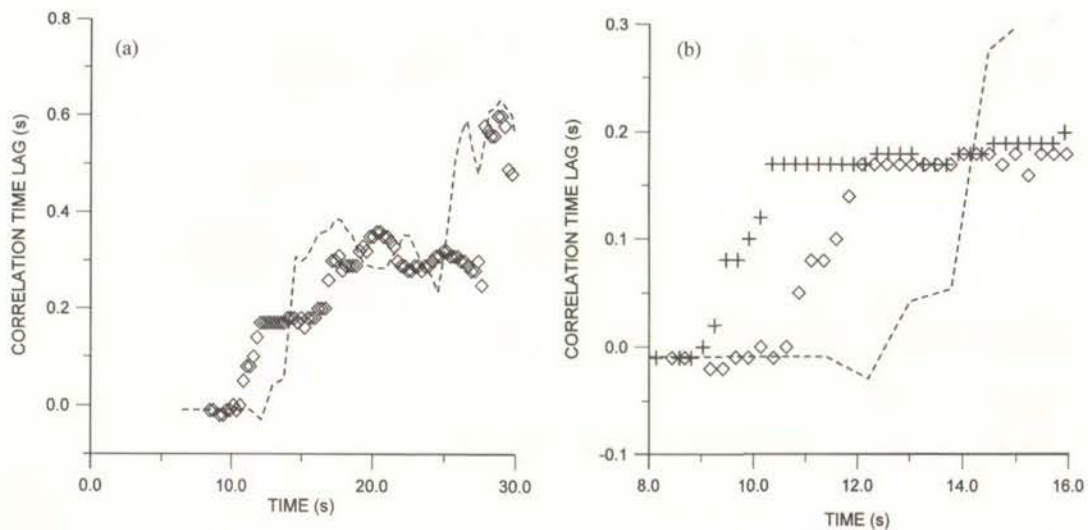


Figure 13. Comparison of time compression and individual window correlation results. (a) Result for 6.4 s window. (b) Comparison of 6.4 s window result (\diamond) with that for 9.6 s window (+).

the root cause of the differences by performing a second individual correlation calculation using a greater window duration. Results are shown on an enlarged time scale in Figure 13(b). The diamond-shaped data points are identical to those shown in Figure 13(a) for the 6.4 s window. The + data points correspond to the second calculation using a window width of 9.6 s. The

dashed line shows the time compression result. The striking point about this figure is the similar shape but different timing exhibited by the two individual correlation results. The 9.6 s window data show the first strong softening occurring between 9.4 and 10.5 s. The same effect does not appear for the 6.4 s window until roughly 10.7 s, and it ends at about 12 s. The reason for this becomes clear when one inspects the original acceleration records. Referring to Figure 3, note the ground surface acceleration peaks marked *A* and *B*. These occur at roughly 14.0 and 15.1 s. The 6.4 s window will just begin to encompass peak *A* when the centre of the window lies at $14.0\text{ s} - 3.2\text{ s} = 10.8\text{ s}$. It will encompass peak *B* when its centre lies at $15.1\text{ s} - 3.2\text{ s} = 11.9\text{ s}$. These times almost exactly coincide with the times for the softening indicated by the diamond-shaped points in Figure 13(b). The longer window duration of 9.6 s encounters the peaks somewhat earlier. The exact time difference will be $4.8\text{ s} - 3.2\text{ s} = 1.2\text{ s}$, and this is nearly exactly the time separating the two correlation results. It is evident that using individual time windows in this way may lead to flawed understanding. The lag time is dominated by the major peaks of the acceleration record, to the extent that the correlation result is instantaneously skewed as soon as the peak enters the window.

Next, we consider the North-South component for the 0 and 16 m depth instruments. The 12 s – 20 s segment of the North-South acceleration record is illustrated in Figure 14. As before, visual inspection suggests the records are correlated although the correlation is not so clear cut as in Figure 3. If we carry out the time compression algorithm here, the before and after correlation graphs are found in Figure 15. Before time compression the peak correlation lag was 0.37 s. After time compression it is reduced to 0.08 s, slightly larger than the value of 0.07 s found for the East-West records. The cumulative time compression is also somewhat different in this case. It is shown in Figure 16. The East-West cumulative compression from Figure 9 is shown there also as a dashed line. Both results were obtained using the $(t_F - t_S)$ interval of 0.8 s. It is evident from Figure 16 both the North-South and East-West records are in broad agreement. Both suffer dramatic time compression around 14 s and both have a final cumulative compression value near 0.3 s. However, the North-South record does not reveal the dramatic increase and decrease in

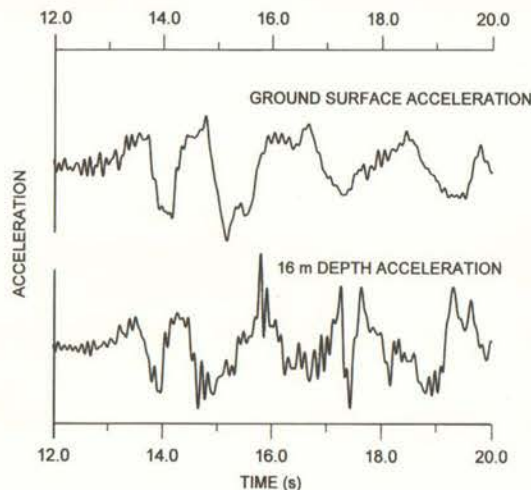


Figure 14. Part of the North-South Port Island acceleration records from 0 and 16 m depths.

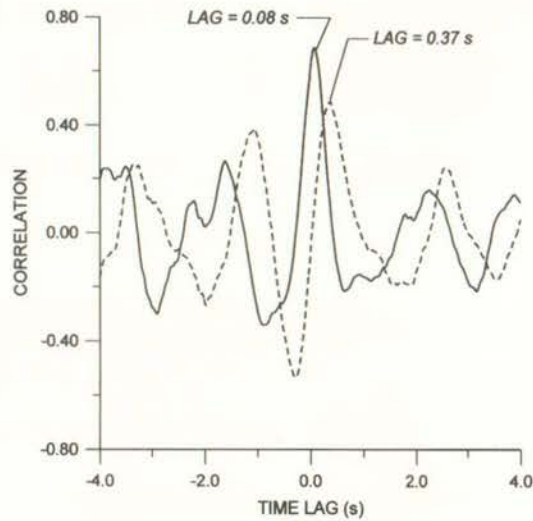


Figure 15. Correlation of Port Island North-South data from 0 and 16 m: dashed line shows correlation of original data; solid line shows correlation after time compression.

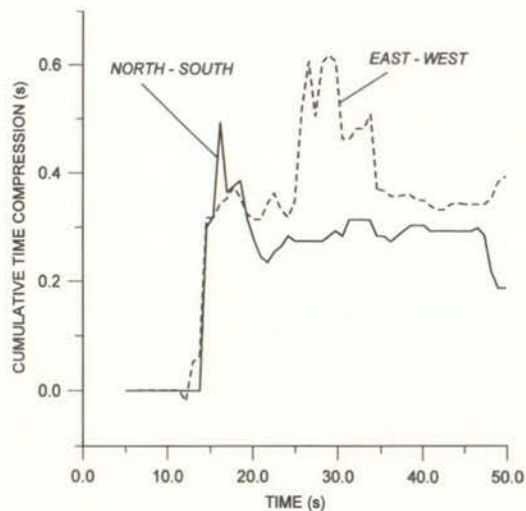


Figure 16. Cumulative time compression curves: solid line for North-South data, dashed line for East-West data.

time compression found between 25 and 35 s on the East-West record. Realising that the cumulative time compression is inversely proportional to the shear modulus, the differences in time compression may suggest anisotropic effects may be present. However, they are of a transient nature, and the soil appears to be more or less isotropic at the conclusion of shaking. This is consistent with the surmise that much of the softening results from increased pore pressure and liquefaction effects.

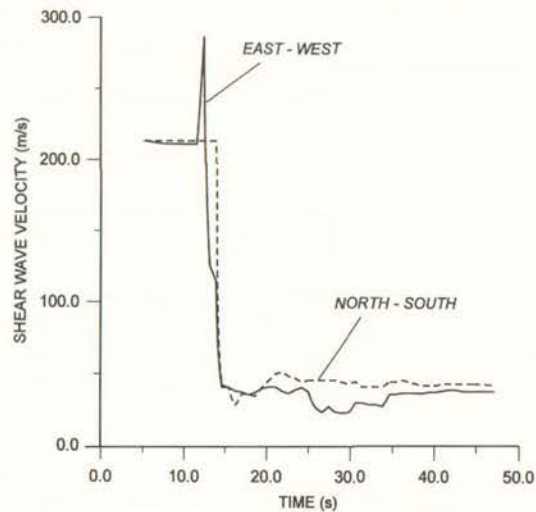


Figure 17. Estimated average shear wave velocity between 0 and 16 m depth at Port Island. Solid line results from East–West records, dashed line from North–South records.

Note that the North–South and East–West records give different estimates for the small deformation elastic lag time. The average of the two values is 0.075 s. Using this average value for t_0 , two curves for shear wave velocity based on Equation (7) are shown in Figure 17. The solid line refers to the East–West data, the dashed line to the North–South data. Note the relatively muted effect of the transient jump in time compression between 25 and 35 s on the East–West record. The peculiar spike in the East–West response at about 12 s is caused by the slight time stretching that occurs at that time in Figure 9(a).

This time stretching is not thought to be representative, but it does have a dramatic effect on the shear wave velocity calculation as can be seen from Equation (7). With t_0 equal to 0.075 s, the negative value for C_m equal to -0.019 s results in a shear wave velocity of 286 m/s. This is not considered realistic. We can offer no explanation for the time stretching at 11 s, but it seems highly unlikely stiffening would occur at this point in the record.

Finally, we note that seismic profiling was carried out at the Kobe site to estimate the small deformation shear wave velocity structure. As reported by Iwasaki and Tai [2], the uppermost 5 m soil segment was assigned a velocity of 170 m/s while in the segment between 5 and 19 m the shear wave velocity was found to be 210 m/s. This suggests a small deformation shear wave velocity for the 0–16 m depth of 198 m/s. This value is close to the initial shear wave velocity of $16\text{ m}/0.075\text{ s} = 213\text{ m/s}$ obtained from the average of the time compression results for the East–West and North–South records.

DISCUSSION

The time compression algorithm presented here possesses several advantages for estimation of shear modulus or shear wave velocity from downhole acceleration records. First, the algorithm is

physically appealing. The idea of time compression bringing the upper acceleration record into closer correlation with the lower is easily grasped and acted on. The algorithm is also computationally efficient. For both the East-West and North-South Port Island records discussed above, the complete calculation time on a 133 MHz Pentium PC did not exceed 150 s. Another advantage is the ability of the algorithm to be used repetitively. If one questions the result of the first time compression computation, a second application will quickly show whether the initial result was accurate or not.

Numerical solutions of optimization problems are often delicate calculations. In the present case we have a large multivariate problem, the dimension of the optimization being equal to M , the number of time intervals for compression. Fortunately, it is not required to *simultaneously* optimise all the Δ_m 's; nevertheless, the 'lumpy mattress' effect may still exist for this problem and it may create difficulties in some circumstances. For example, one can envision a pathological situation in which the calculated time compression Δ_m is greater than the segment size. This would imply time is inverted in the segment, not a possibility that could be entertained in any circumstances. Fortunately, the algorithm developed here appears to be quite robust in this regard. The Kobe records clearly represent a severe test, yet the calculations presented above were performed without excessive care and the results appear to be consistent and sensible.

The comparison between time compression and segmental correlation results shows clearly that the two methods are not equivalent. Time compression leads to distinctly different results, and, for the Kobe records, one can argue that time compression gives a significantly more accurate picture of the time at which softening occurred.

Finally, note that Figure 16 shows broad agreement between the East-West and North-South records, particularly near the end of shaking where both calculations suggest little additional softening is occurring. Time compression appears to give a consistent result for both sets of records. Also the small deformation time lags agree closely in both cases, and provide an estimate for the elastic shear wave velocity that is in reasonable agreement with the value obtained from seismic profiling.

ACKNOWLEDGEMENTS

This study was funded by the New Zealand Earthquake Commission Research Foundation under project number 99/345. Grateful thanks are expressed to Dr Yoshinori Iwasaki and the Committee of Earthquake Observation and Research in the Kansai Area (CEORKA) for making the Port Island records available for this study. Thanks are also accorded to two anonymous reviewers of the original version of the paper. Their comments led to significant improvements in computational algorithm.

REFERENCES

1. Ishihara K, Muroi T, Towhata I. In-situ pore water pressures and ground motions during the 1987 Chiba-Toho-Oki earthquake. *Soils and Foundations* 1989; **29**(4):75-90.
2. Iwasaki Y, Tai M. Strong motion records at Kobe Port Island. *Soils and Foundations* (Special Issue: Kobe) 1996; 29-40.
3. Zeghal M, Elgamel A-W. Analysis of site liquefaction using earthquake records. *Journal of Geotechnical Engineering ASCE* 1994; **120**:996-1017.
4. Elgamel A-W, Zeghal M, Tang HT, Stepp JC. Lotung downhole seismic array. I: Evaluation of site dynamic properties. *Journal of Geotechnical Engineering ASCE* 1994; **121**:350-362.
5. Zeghal M, Elgamel A-W, Tang HT, Stepp JC. Lotung downhole array. II: Evaluation of soil nonlinear properties. *Journal of Geotechnical Engineering ASCE* 1994; **121**:363-378.

6. Chang C-Y, Mok CM, Power MS, Tang YK, Tang HT, Stepp JC. Development of shear modulus reduction curves based on Lotung ground motion data. *Proceeding of the 2nd International Conference on Recent Adv. Geotech. Earthquake Engineering Soil Dyn.*, St Louis, 1991; 111-118.
7. Wen K-L, Beresnev IA, Yeh YT. Investigation of non-linear site amplification at two downhole strong ground motion arrays in Taiwan. *Earthquake Engineering Structural and Dynamics* 1995; **24**:313-324.
8. Li XS, Shen CK, Wang ZL. Fully coupled site response analysis for 1986 Lotung earthquake. *Journal of Geotechnical Engineering ASCE* 1998; **124**:560-573.
9. Kazama M. Nonlinear dynamic behavior of the ground inferred from strong motion array records at Kobe Port Island during the 1995 Hyogo-Ken Nanbu earthquake. *Proceedings of the International Workshop on Site Response*, Yokosuka, Japan, Vol. 2, 1996; 185-199.
10. Seed HB, Idriss IM. *Soil moduli and damping factors for dynamic response analyses*. Earthquake Engineering Research Report *EERC 70-10*, University of California, Berkeley, 1970.
11. Bendat JS, Piersol AG. *Engineering Application of Correlation and Spectral Analysis*. Wiley. New York, 1980.
12. Elgamal A-W, Zeghal M, Parra E. Liquefaction of reclaimed land in Kobe, Japan. *Journal of Geotechnical Engineering*, ASCE 1996; **122**(1):39-49.
13. Press WH, Flannery BP, Teukolsky SA, Vetterling WT. *Numerical Recipes. The Art of Scientific Computing*. Cambridge Press: New York, 1988.

Soils and Seismology

Research Engineering



RESEARCH REPORT

**ESTIMATION OF SOIL SHEAR MODULUS SOFTENING
DURING STRONG GROUND SHAKING
USING GROUND SURFACE AND DOWNHOLE
ACCELERATION RECORDINGS**

By

**R.O. Davis and J.B. Berrill
Soils and Seismology
P.O. Box 29-336
Christchurch**

March 2000

**ESTIMATION OF SOIL SHEAR MODULUS SOFTENING
DURING STRONG GROUND SHAKING
USING GROUND SURFACE AND DOWNHOLE
ACCELERATION RECORDINGS**

Report prepared for the
Earthquake Commission Research Foundation

Project Number 99/345

By

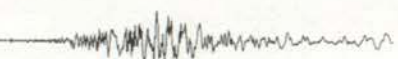
R.O. Davis and J.B. Berrill
Soils and Seismology
P.O. Box 29-336
Christchurch

March 2000



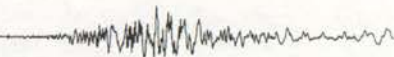
PREFACE

This report describes work carried out under EQC Research Foundation Project 99/345: *Estimation of shear modulus softening based on downhole acceleration data*. The authors are grateful for the support of the Research Foundation as well as for assistance provided by several international colleagues. In particular, thanks are expressed to Dr. Yoshinori Iwasaki and the Committee of Earthquake Observation and Research in the Kansai Area (CEORKA) for making the Kobe Port Island records available for this study and to Professor Ralph Archuleta for providing the Superstition Hills and Elmore Ranch earthquake data.



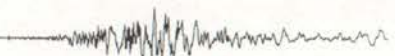
ABSTRACT

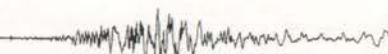
A growing number of earthquakes have occurred close to downhole accelerometer arrays. The resulting acceleration records from different depths provide valuable insight into the propagation and amplification of seismic waves in the site soils. Interpretation of data from these events frequently involves estimation of shear modulus for the soils involved. While estimates for small strain elastic deformations are usually available, softening due to nonlinear soil behaviour introduces unwanted complications in any estimation of shear moduli during strong shaking. A commonly used approach is to model the soil column as a one-dimensional shear beam and adjust the soil parameters throughout the period of shaking to best fit the observed data. The method is both awkward and unreliable since the shear beam model presupposes the form of response for the soil system. An improved method that directly uses the cross-correlation of acceleration records is proposed here. The research described in this report develops an algorithm for estimating the average shear modulus directly from measured acceleration data at different depths. The algorithm relies on cross-correlation of two records together with time compression of one of the records to automatically estimate the average shear wave velocity as a continuous function of time while shaking progresses.



CONTENTS

SECTION	PAGE
Introduction	1
Background	4
Method of Analysis	8
Case Histories	13
Kobe Port Island	13
Elmore Ranch	21
Superstition Hills	26
Summary and Recommendations for Future Work	34
References	36
Appendix A	38
Appendix B	40





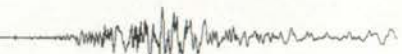
INTRODUCTION

Vertical arrays of accelerometers spaced at intervals of from five to twenty or more metres have been placed at a number of sites throughout the world [References 1 – 4]. They are generally referred to as downhole arrays. Their central purpose is to provide direct measurement of site amplification effects. The resulting acceleration records from different depths provide valuable insight into the propagation and modification of seismic waves in the site soils. Interpretation of data from a recorded event is relatively straightforward for small or distant earthquakes where the ground deformation is relatively small and elastic behaviour predominates. In these cases investigators normally model the soil response using vertically propagating SH waves. There is a requirement of course for shear moduli values in order to specify shear wave velocities. Estimates of shear modulus for the soils involved may be obtained by several means including laboratory tests, field seismic profiling, or time series correlation of the downhole records themselves.

Shear moduli are not so easily estimated for stronger earthquakes when softening due to nonlinear soil behaviour may introduce unwanted complications. In stronger events the site soils may undergo progressive changes depending on the levels of stress and strain and (for saturated soils) pore pressure increase. It is not nearly so easy to estimate shear moduli for these circumstances. Clearly field seismic profiling is inappropriate as only small strain deformations are involved. Laboratory tests can be adapted to simulate the estimated stress history, but there are obvious difficulties in synthesizing an appropriate stress history and then implementing it in the lab.

Often, time series correlation of downhole acceleration records from two depths has been used to estimate the average velocity of waves propagating between those depths. The time series correlation directly provides an estimate for the lag or travel time for waves to propagate from the lower depth to the higher. The wave velocity is obtained by dividing the distance between instruments by the peak correlation lag time. Wave velocities can then be easily translated into modulus values. This method is clearly appropriate, provided the level of ground motion is not sufficiently strong to result in significant nonlinear soil behaviour. As an example, Elgamal, *et al.* [4] used time series correlation for a variety of small earthquakes to assess the shear wave velocity structure at the SMART1 Lotung downhole test site in Taiwan. The data developed in [4] was later used in the analysis of stronger motion data from larger earthquakes at the test site [5].

Problems arise with correlation of records when stronger levels of shaking occur. In those cases, early parts of the acceleration history will correspond to the generally stiffer small deformation moduli values that initially exist at the site. As shaking progresses the moduli may soften and the wave travel time between the instrument locations in the downhole array will lengthen. This lengthening may be significant whenever the shaking is sufficiently strong to generate nonlinear effects. If one now correlates the two entire records, the calculated lag will reflect neither the initial



small deformation behaviour nor the later softened behaviour. Instead one obtains an average lag lying somewhere between the initial and softened values. Several investigators have used a variety of methods to overcome this difficulty. Resonant frequencies determined from Fourier spectral ratios were used by Chang, *et al.* [6] to estimate shear wave velocities at the Lotung SMART 1 array. A similar analysis was carried out by Wen, *et al.* [7]. In a separate efforts, Li, *et al.* [8] employed a sophisticated hypoplasticity model to numerically simulate ground motion at the Lotung site, while Kazama [9] directly approximated shear stress and strain for the Kobe Port Island downhole acceleration records. None of these methods enjoy the simplicity and directness associated with simple correlation of two downhole records.

This report attempts to overcome the problem described above. Consider the typical two-instrument downhole array sketched in Figure 1. It is desired to obtain a continuous history of shear wave velocity (or the corresponding shear modulus) throughout the times where shaking and softening occur. We will present a technique for compressing the time scale of the upper acceleration time history in such a way as to precisely counteract the effects of softening. The new, compressed acceleration history will represent the soil response without softening effects. Its correlation with the buried instrument record will approximate the small deformation response of the intervening soils just as would be the case if no softening had occurred. Meanwhile, the amount of time compression suffered by the upper record will tell us how much softening has occurred and when it occurred. It will be possible to construct a complete picture of the average shear wave velocity between the two instrument levels throughout the duration of the earthquake.

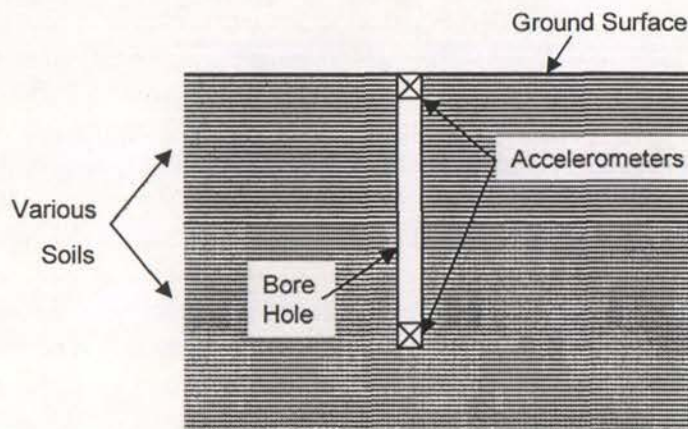
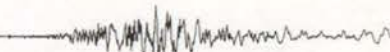


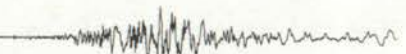
Figure 1. Typical downhole accelerometer array

There are several possible applications for the softened shear modulus history. One can directly compare field softening data with published models for shear modulus reduction such as given by Seed, *et al.* [10]. In instances where liquefaction has been observed, the softening history may give considerable insight into both the onset of liquefaction and the later solidification process. Comparison and verification of analytical site amplification models are possible as well.

The algorithm developed below is reasonably robust. It provides as much detail as the user requires, consistent with the digitisation time scale for the acceleration



records and the distance between the downhole instruments. The digitisation time scale places well defined limits on the accuracy of any approximation for site shear wave velocity. This point is discussed in Appendix A. The time compression method will be illustrated by considering three case histories that cover a range of possible applications. At one extreme the response of the Imperial Valley Wildlife Refuge site to the Elmore Ranch earthquake will be considered. This was a relatively small earthquake and no softening is thought to have occurred. At the other extreme we will consider downhole results from the Port Island array at Kobe where severe softening and liquefaction occurred. We will also consider the response of the Wildlife site to the Superstition Hills earthquake where liquefaction also occurred. All three events present difficulties for the time compression algorithm but sensible results are found in most aspects of each earthquake.



BACKGROUND

The basic elements of our method are most easily described by reference to a specific earthquake. We will begin by considering the Hyogo-ken Nambu or Kobe earthquake of 17 January 1995. A particularly interesting site near Kobe was the reclaimed land known as Port Island. The land was reclaimed by bottom dumping sand and gravel in roughly 15 m deep water over a period of several years beginning in 1966. In 1991 four three-component accelerometers connected to a common trigger were installed in a bore at depths of zero, 16, 32 and 83 meters. A complete set of records were obtained from the Hyogo-ken Nambu earthquake.

Port Island East-West accelerations from the 0 and 16 m depths are illustrated in Figure 2. The aim of this report is to estimate the average shear modulus, or equivalently the shear wave velocity, in the soil between the two instruments, *continuously* throughout the earthquake. Liquefaction was observed at this site and it is clear significant softening occurred during the earthquake.

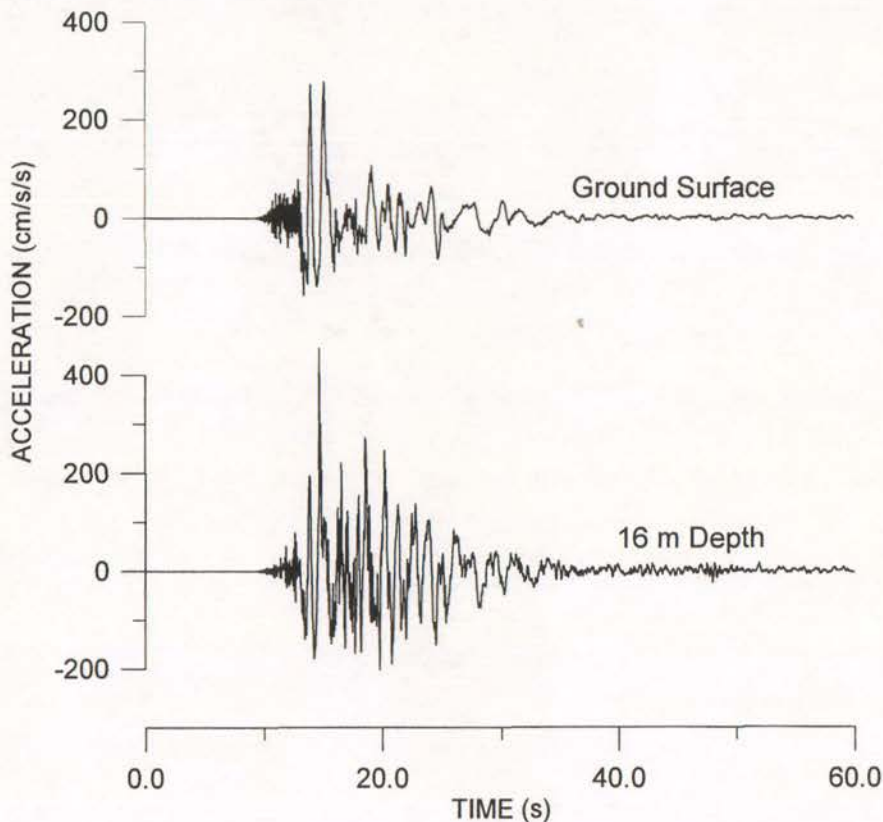
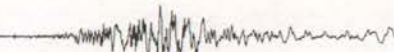


Figure 2. Kobe Port Island acceleration records. East-West data from 0 and 16 m depths.



The full sixty seconds of shaking shown in Figure 2 is difficult to consider in detail because of the small time scale necessitated by the size of the figure. A more informative picture is developed if we expand the time scale. This has been done in Figure 3 where the time interval between 12 and 20 seconds has been isolated. It is clear from this figure that marked correlation exists between the two records. The wave crests denoted A, B and C strongly suggest upward propagating shear waves that, with only minor changes of wave form, move from the 16 m depth to the soil surface. However closer inspection shows that the lag times associated with the three wave crests are significantly different. Examining the digitised records, we find the lag for peak A is 0.17 s, for peak B it is 0.46 s, and for peak C, 0.61 s. The increasing time lag results from the extreme softening of the site during the time interval shown in Figure 3.

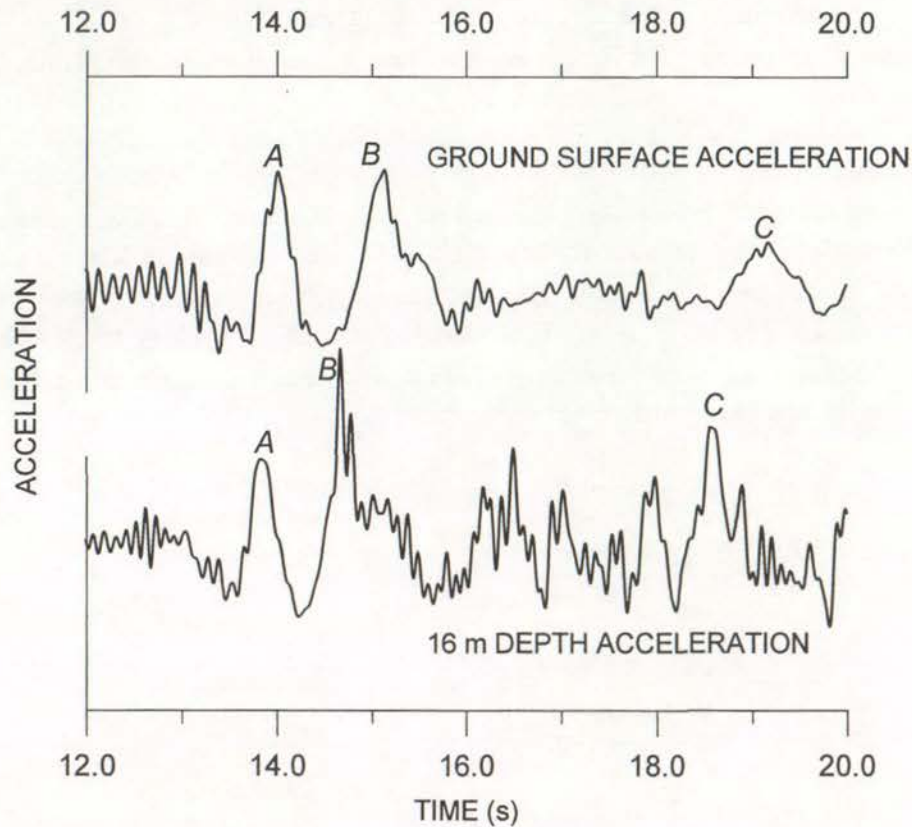
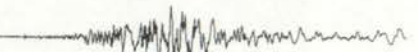


Figure 3. Expanded segment of data from Figure 2.

We can attempt to better understand the Kobe response by examining the correlation of the two records. The discrete time series correlation of two sampled functions $a_k = a(t_k)$ and $b_k = b(t_k)$ is defined as [11]

$$\Gamma(t_m) = \sum_k b_{k+m} a_k \quad (1)$$

where the sum is taken over the entire record. Often Γ is given in normalised form,



$$\Gamma_n(t_m) = \frac{\Gamma(t_m)}{\left(\sum_k a_k^2\right)^{\frac{1}{2}} \left(\sum_k b_k^2\right)^{\frac{1}{2}}} \quad (2)$$

Direct calculation of Γ using equation (1) can be seriously time consuming for long records. In practice one uses the discrete correlation theorem which states that Γ is one member of the discrete Fourier transform pair

$$\Gamma(t_k) \leftrightarrow B_k A_k^* \quad (3)$$

Here A_k and B_k are the discrete Fourier transforms of a_k and b_k and $*$ denotes complex conjugation. A_k and B_k are found using fast Fourier transforms of the given data. The inverse FFT is then used to find Γ . The resulting calculation is extremely efficient.

The functions Γ and Γ_n will both show a peak at the value corresponding to a particular lag or time delay between the two records. The normalised correlation for the two Port Island records is shown in Figure 4. We see a strong peak at $t = 0.31s$. This is the calculated lag for the two records. The corresponding shear wave velocity is $16m/0.31s = 51.6m/s$. This value is, at best, an average wave velocity for the entire time interval of the record. It cannot represent the softening behaviour of the site soils as shaking progresses.

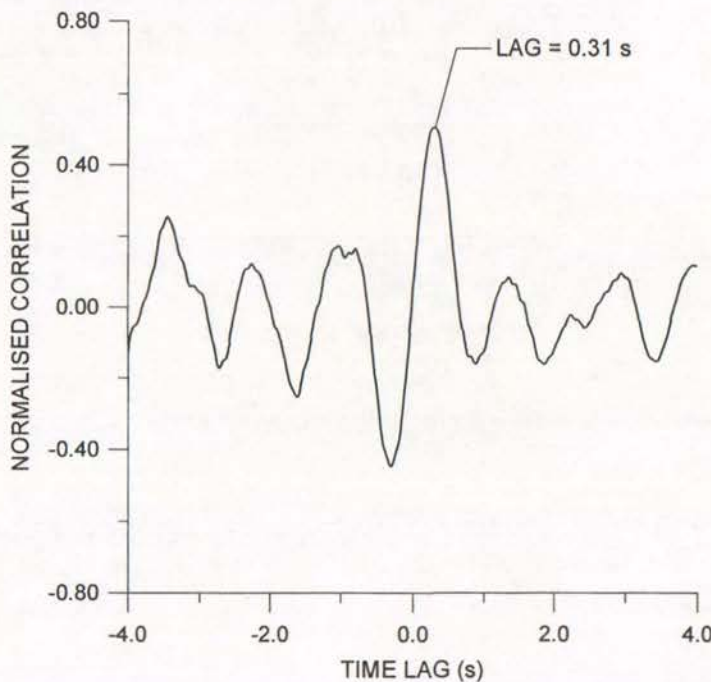
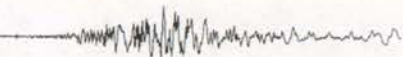
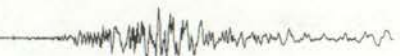


Figure 4. Normalised correlation of East-West Port Island Records



One approach to dealing with softened records such as Kobe is to break down the two records into distinct windows and consider the individual correlations for each window. This was done for the Kobe records by Elgamal, *et al.* [12]. Their results indicate a dramatic reduction in soil stiffness, but lack fine detail regarding the continuous variation of shear wave velocity or shear modulus. The basic problem with this method lies in the size of the record segments to be used. The segments must be sufficiently large to be representative of some part of the record. The resulting lag is a single number associated in some (not fully specified) way with the segment. If the segment is made too small, the desired correlation will often be lost and spurious values for the lag may result. We will compare this method with the proposed algorithm later in the report.



METHOD OF ANALYSIS

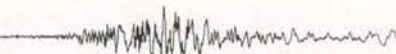
Our aim in this report is to use the correlation of two downhole acceleration records as a tool to lead to a continuous picture of shear wave velocity variation during an earthquake. The basic idea will be to maximise the correlation of the records by nonlinearly compressing the time scale of the upper acceleration record. Referring again to Figure 3, it is clear that compressing the time scale of the upper record in some appropriate way could lead to better correlation of the two records. If the correct amount of time compression were put in place, the increasing lag associated with wave crests B and C could be completely eliminated and all three peaks could have the same lag. The effect on the correlation function Γ shown in Figure 4 would be twofold: first the peak at 0.31 s would be shifted to the left, second the magnitude of the correlation peak would be increased. This suggests that we could use the magnitude of the peak value of Γ as a criterion for adjusting the time scale of the upper record.

Next, we realise that if the time scale is compressed, the amount of compression necessary to maximise the correlation will be equal to the amount by which softening of the site soil has lengthened the travel time between the two instruments. If we divide the distance between the instruments by the sum of the travel time for small deformation elastic waves plus the amount of time compression, the result should be the shear wave velocity corresponding to the softened soil profile. This is the basic idea of our algorithm.

In more detail, we proceed as follows. Suppose we have two sampled acceleration records denoted a_k and b_k such as those shown in Figure 2. Let a_k be the record from the higher instrument. Also, let the time corresponding to a_k and b_k be t_k , and assume the time increment δt between samples is a constant. Now consider a new time scale denoted \hat{t}_k where time is compressed in some segment of the record. We define \hat{t}_k as follows

$$\hat{t}_k = \begin{cases} t_k & \text{for } t_k \leq t_S \\ t_k - \Delta \left(\frac{t_k - t_S}{t_F - t_S} \right) & \text{for } t_S < t_k \leq t_F \\ t_k - \Delta & \text{for } t_F < t_k \end{cases} \quad (4)$$

Here \hat{t}_k is the compressed time, t_S and t_F are the start and finish times for the compressed segment, and Δ is the total amount of compression at the end of the segment. Time is compressed linearly between t_S and t_F and we continue throughout the remainder of the record using a constant time translation Δ . An



example of a compressed time scale is shown schematically in Figure 5. In the figure the compression Δ has been taken as 0.50 s and the values of t_S and t_F are 14.0 s and 16.0 s. The new compressed time is shown by the solid line while the dashed 45 degree line is simply a plot to the original time versus itself. Note that the new compressed time \hat{t}_k will no longer have a constant increment size δt on the interval $[t_S, t_F]$ and the values of \hat{t}_k and t_k will generally be different for all times greater than t_S .

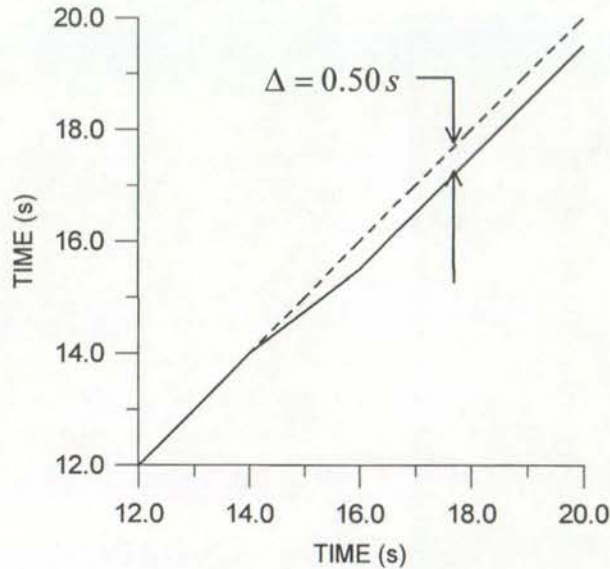


Figure 5. Example of compressed time scale.

Next, we rewrite the upper acceleration record, interpolating the values of acceleration at the appropriate times in the newly compressed time scale. In this way we realign the new compressed acceleration record with the original sampling times. This is necessary in order that we can carry out the correlation of the new record with the original b_k acceleration record. We rewrite the record as follows. For any desired value of time t_j in the original time base, we find the corresponding acceleration using linear interpolation

$$\hat{a}_j = a_k + (a_{k+1} - a_k) \left(\frac{t_j - \hat{t}_k}{\hat{t}_{k+1} - \hat{t}_k} \right) \quad (5)$$

Here \hat{a}_j is the new interpolated acceleration at time t_j , \hat{t}_k is compressed time, a_k is the acceleration corresponding to \hat{t}_k . The index k is selected so that $\hat{t}_k \leq t_j \leq \hat{t}_{k+1}$. It is a simple matter to sweep through the compressed record interpolating the new acceleration values. The results of this effort are new accelerations based on the compressed time scale, but now properly aligned with the original time base. An example is illustrated in Figure 6. The time interval for compression is defined by $t_S = 14.0$ s and $t_F = 16.0$ s. For purposes of illustration, the value of Δ has been set equal to 0.25 s. In practice, the value of Δ will be determined by maximising the



correlation. Also, the interval to be compressed may be considerably shorter than 2 seconds, but a large value is useful here to illustrate the concepts involved. In Figure 6 the dashed line is the original acceleration record and the solid line the compressed record. Note how the compression is initiated at $t_s = 14.0s$ and how the amount of compression remains constant for times greater than $t_F = 16.0s$.

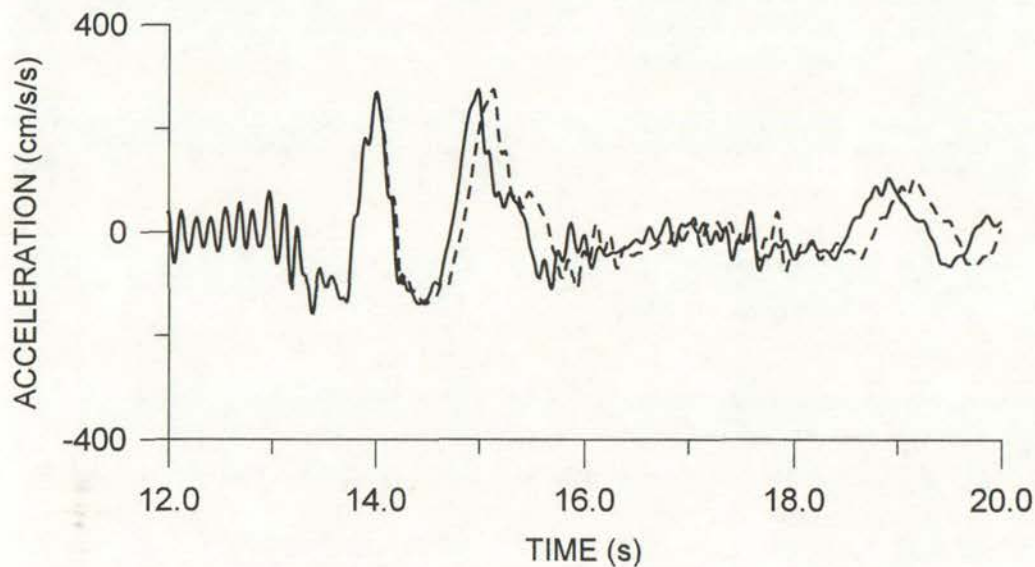


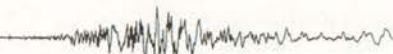
Figure 6. Example of effect of compressed time on ground surface accelerations.

Our algorithm for estimating shear wave velocity is outlined in Figure 7. We begin by partitioning the time scale for the complete record into M segments $(t_F - t_S)$ of equal size. Then beginning with segment one, we maximise the peak value of the correlation Γ by adjusting the value of the compression Δ_1 . Note that the correlation is made using the entire record. The compression of segment one not only affects the record within the segment but also at all later times. We then move forward to segment 2, maximising Γ to find Δ_2 , and so on through the record, stopping only when the shaking becomes too weak to be of interest or when the values of Δ_m become very small in comparison to the segment size. Next, we note the Δ_m 's for each segment have a cumulative effect on all the record that follows. Therefore we construct the cumulative time compression C_m according to

$$C_m = \sum_{i=1}^m \Delta_i, \quad m = 1, 2, \dots, M \quad (6)$$

The value of C_m represents the time compression required to offset the softening effect caused by strong shaking in the soil up to the time corresponding to the end of segment m .

Once time compression is complete, the two acceleration records will be correlated with a lag time corresponding to the initial small deformation shear modulus of the



soil before softening commenced. This lag can be read off the final correlation. Let its value be t_0 . We can now construct the shear wave velocity history as

$$v_s(t_m) = \frac{\text{distance between instruments}}{t_0 + C_m} \quad (7)$$

Here t_m denotes the time at the end of segment m .

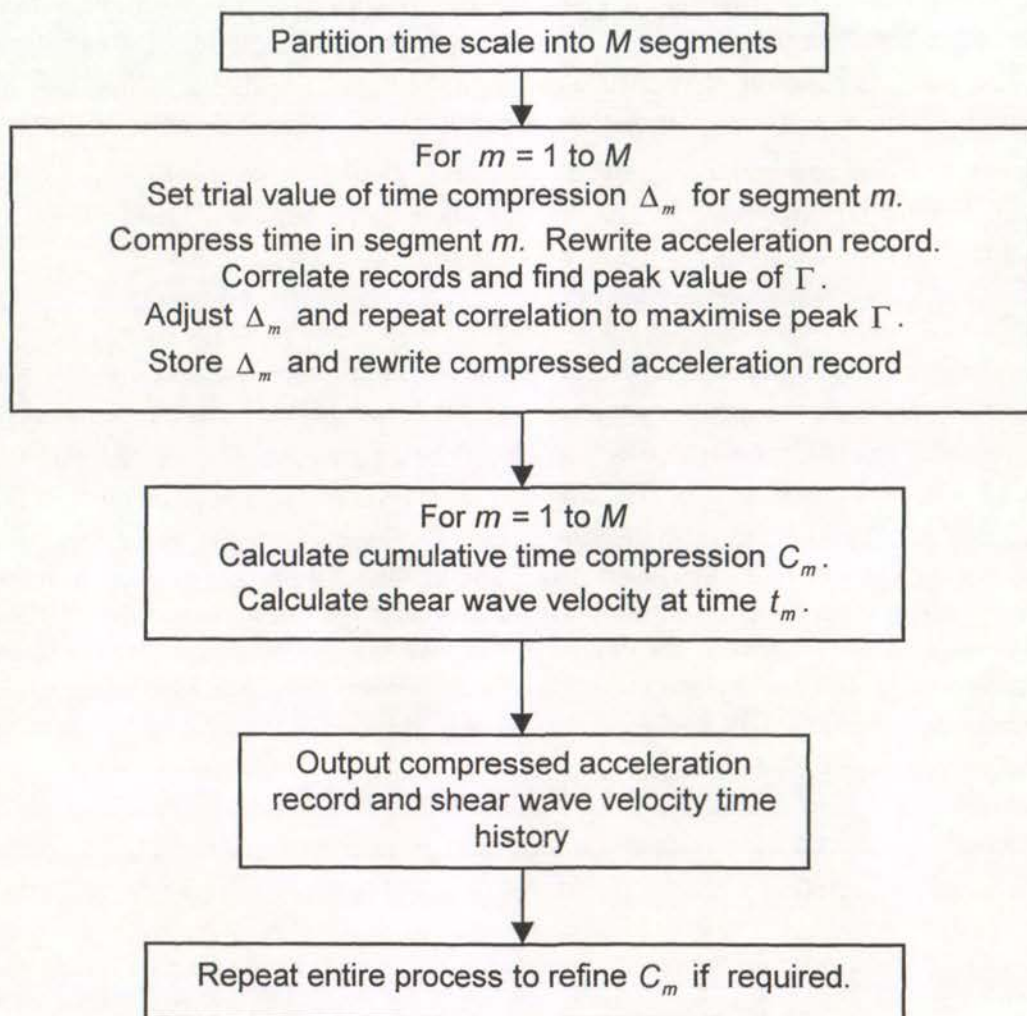
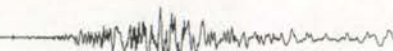


Figure 7. Flow diagram for time compression algorithm.

In the next section we will show some typical applications using the Kobe Port Island and USGS Wildlife records. However, before doing this, three points should be noted. The first concerns the problem of optimising the magnitude of the correlation peak by adjusting the value of the time compression Δ_m for segment m . This is a relatively simple one-dimensional optimisation problem. Several different optimising schemes were tried while the algorithm was under development. The most effective, from the standpoint of being both straightforward and highly stable, was the golden section algorithm. The subroutines GOLDEN and MBRAK from



Numerical Recipes in Fortran [Press, et al., 13] were employed directly. The MBRAK routine first brackets the optimal compression value. Then GOLDEN refines the value to within the desired tolerance. For the case histories described below, the tolerance was set equal to $0.01s$, the value of the digitisation time interval for the Kobe acceleration records. A complete FORTRAN listing of the algorithm is given in Appendix B.

The second point to note here is that the entire algorithm outlined above may be repeated. That is, the fully compressed record emerging at the conclusion of the optimisation may be reused as if nothing had occurred. The result is a new cumulative time compression, say C'_m . We may then sum C_m and C'_m to obtain a refined time compression. Experience suggests the best procedure is to first run the algorithm with a relatively large time interval $(t_F - t_S)$ and then to repeat the process with the time interval halved. A third calculation, with $(t_F - t_S)$ halved again, may be performed and so on. At each stage more detail is added to the time compression record.

Our third comment follows from the second. The magnitude of $(t_F - t_S)$ is of considerable significance to the overall result. If we attempt to make the interval $(t_F - t_S)$ too small, we risk overemphasizing the importance of a small segment of the record. For the case histories considered below, we used an initial interval $(t_F - t_S)$ of either $0.8s$ or $1.6s$. Halving this to interval leads to improvement in the degree of detail embodied in the results. Halving again may yield more detail but does not appear to cause significant improvement. It is important to keep in mind that, at best, we can hope for no more than an accurate representation of the *average* shear wave velocity between the depths of the instruments involved. Other effects such as soil layering, P-waves and surface waves have undoubtedly contaminated the records to some extent and use of an excessively small interval $(t_F - t_S)$ may unduly emphasise their importance.

A second problem can also arise when too small an interval $(t_F - t_S)$ is used. As in almost any optimisation problem, our objective function (the peak correlation value) has multiple extrema. This is sometimes referred to as the bumpy mattress problem. We seek to smoothly follow one extreme value as the algorithm sweeps through the record, but it is always possible to jump to another nearby peak that may temporarily appear more attractive to the program. It is not difficult to identify this phenomenon since, if it occurs, the lag time will undergo a sudden dramatic change. We can generally avoid the problem by using larger intervals $(t_F - t_S)$ since they will generally encompass sufficient wave complexity to preclude an easy path for the optimisation to take to a spurious peak. On the other hand, small intervals may invite a jump to a nearby local extremum. For this reason, as well as the comment above, small time intervals are not recommended.



CASE HISTORIES

In this section we will consider three separate earthquakes. The first is the 1995 Kyogo-ken Nambu earthquake as recorded at Kobe Port Island. We have already used part of this record to illustrate the development of the time compression algorithm above. The second two earthquakes were both recorded at a site in the Imperial Valley, California. They were the 1987 Elmore Ranch earthquake and the 1987 Superstition Hills earthquake.

Kobe Port Island

Consider once again the East-West acceleration records from the ground surface and 16 m depth at Port Island shown in Figures 2 and 3. We have carried out the programme of calculations outlined above using a time interval of 0.8 s. Figure 8 shows the normalised correlation functions Γ_n for the records both before and after time compression. The dashed line in Figure 8 is identical to the correlation shown in Figure 4. The solid line shows the correlation after time compression. From Figure 8, we see that the magnitude of the peak correlation has been significantly improved (from 0.504 to 0.651) by the compression. We also see the lag has been reduced to 0.07 s. This value suggests an initial small deformation shear wave velocity of $16\text{ m}/0.07\text{ s} = 228\text{ m/s}$.

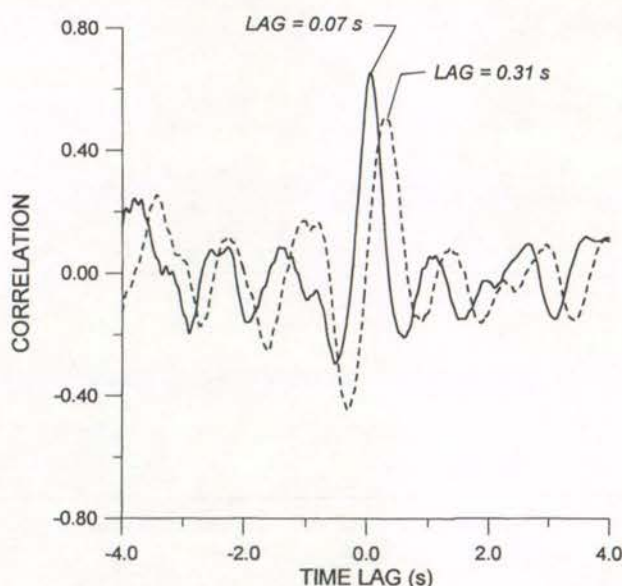
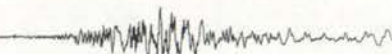


Figure 8. Correlations for Port Island data.

Figure 9a shows the cumulative time compression C_m plotted versus time. The calculation begins at $t = 5\text{ s}$, and for a little more than seven seconds, C_m remains equal to zero. No time compression occurs in this early part of the record. Around 12 seconds there is a slight *stretching* of the time scale, indicated by the small



negative jump in C_m . Then between 13 and 14 seconds a rapid compression is found. This part of the record evidently contains the most marked softening of the site soils. A second episode of softening is evident at 25 seconds, but this is followed by a decrease in C_m indicating stretching of the time scale is required by the algorithm. The computation was stopped at 50 seconds.

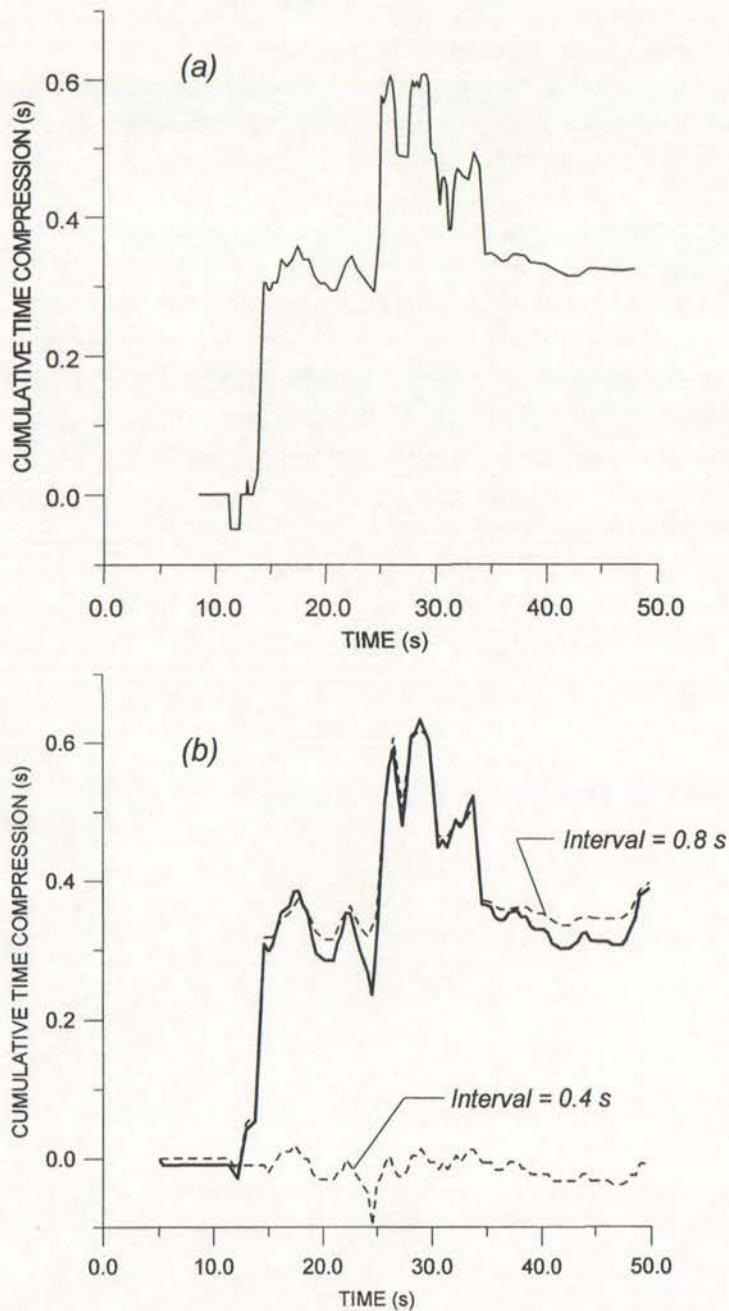
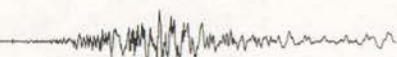


Figure 9. Cumulative time compression for surface accelerations at Port Island.
 (a) Results for 0.8 s intervals. (b) Results after halving the time interval.

Figure 9b illustrates a second time compression, now using an interval ($t_F - t_S$) of 0.4 s. The compressed upper record from the previous calculation is used as input



for this calculation. As one might expect, the resulting time compression is generally small. It is shown by the dashed line hovering around zero compression near the bottom of the figure. The original, 0.8 s interval, cumulative compression is also shown by the second dashed line. The summation of the two lines is shown as the solid line. It seems evident from the figure that additional detail has been added to the original result, but the overall trend in the compression is largely preserved. The magnitude of the peak correlation is increased by this second calculation to a value of 0.692. The lag time remained steady at 0.07 s.

Figure 10 shows the segment of the ground surface acceleration history between 12 and 20 seconds. The dashed line represents the original acceleration history while the solid line shows the compressed history after the above calculations. Significant amounts of time compression are evident near 14 seconds. In Figure 11 we have re-plotted both the upper (compressed) and lower acceleration records, and we have offset the two records by the final lag of 0.07 s. In comparison with Figure 3, it can be seen from this figure how the two records are now visually well correlated.

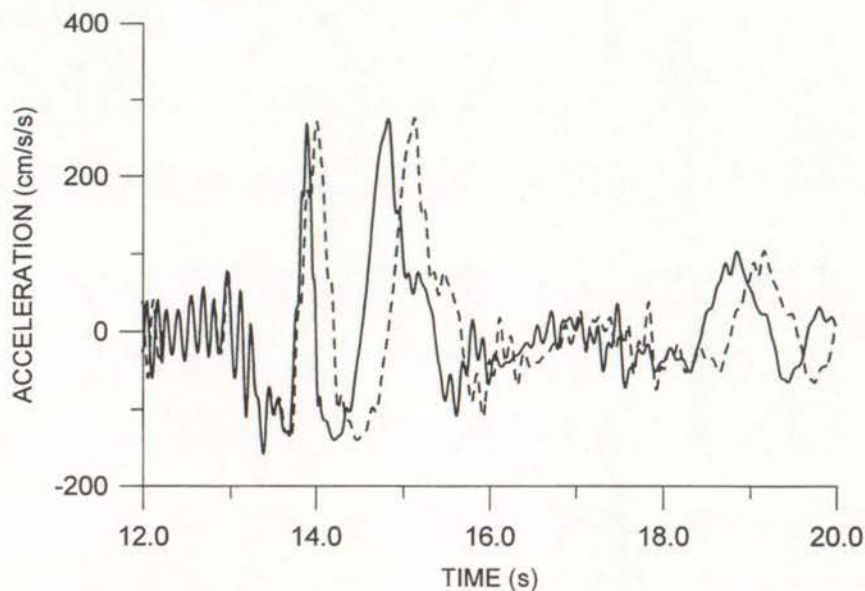
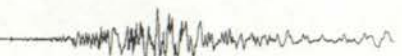


Figure 10. Part of the ground surface acceleration record before and after time compression.

As we noted above, it is possible to continue repeating the calculation with progressively smaller time increments. Figure 12 illustrates the result of this process for intervals of 0.2 s and 0.1 s. The heavy solid line represents the situation following the 0.4 s interval compression. That line is the same as the solid line in Figure 9b. The dashed line shows the result from the 0.2 s compression and the light solid line shows the 0.1 s calculation. Inspecting the figure we see the smaller time intervals tend to exaggerate some of the peaks in the earlier result. The degree of exaggeration is not large, yet one must doubt their validity for the reasons discussed above. The peak correlation is not greatly increased by either of the new calculations. Its value increases to 0.704 for the 0.2 s run, and to 0.706 for the 0.1 s calculation. The lag time remained steady at 0.7 s throughout both calculations.



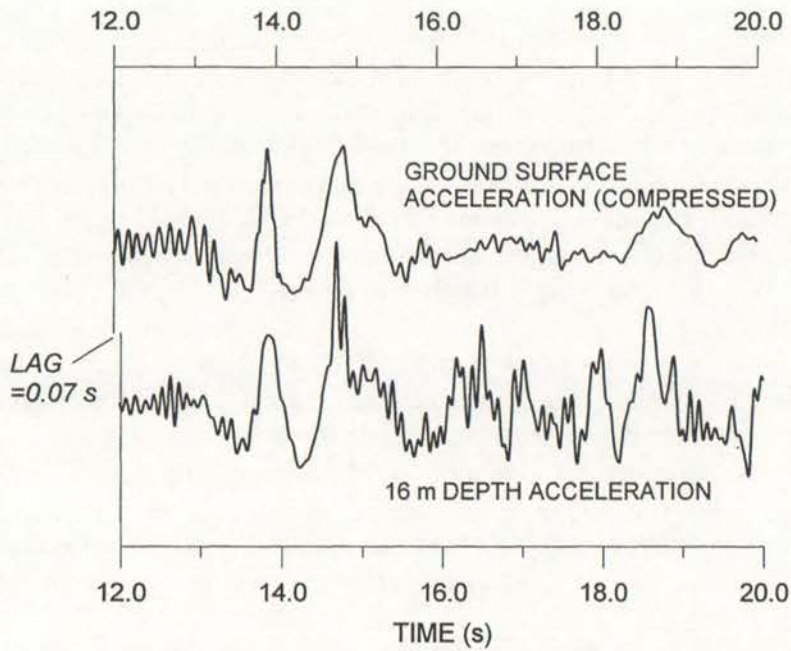


Figure 11. Comparison of 0 and 16 m records after time compression. Note that 16m record is offset by 0.07 s.

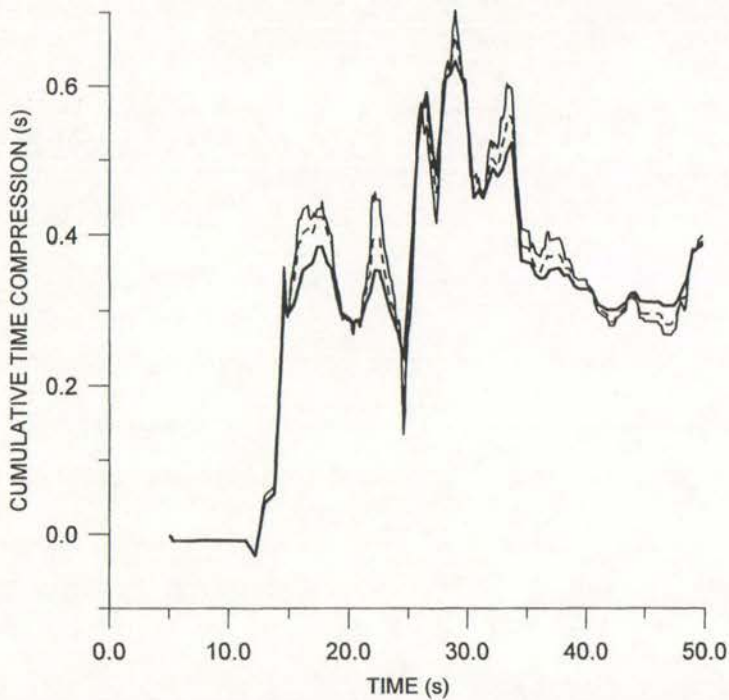


Figure 12. Effect of further halving time interval on cumulative time compression. Heavy solid line is identical to Figure 9. Dashed line corresponds to 0.2 s intervals, light solid line to 0.1 s intervals.

As mentioned above, another approach to our problem is individually correlating the two records over individual time windows. Figure 13a shows results from such a computation. The diamond shaped data points on the figure represent lag times



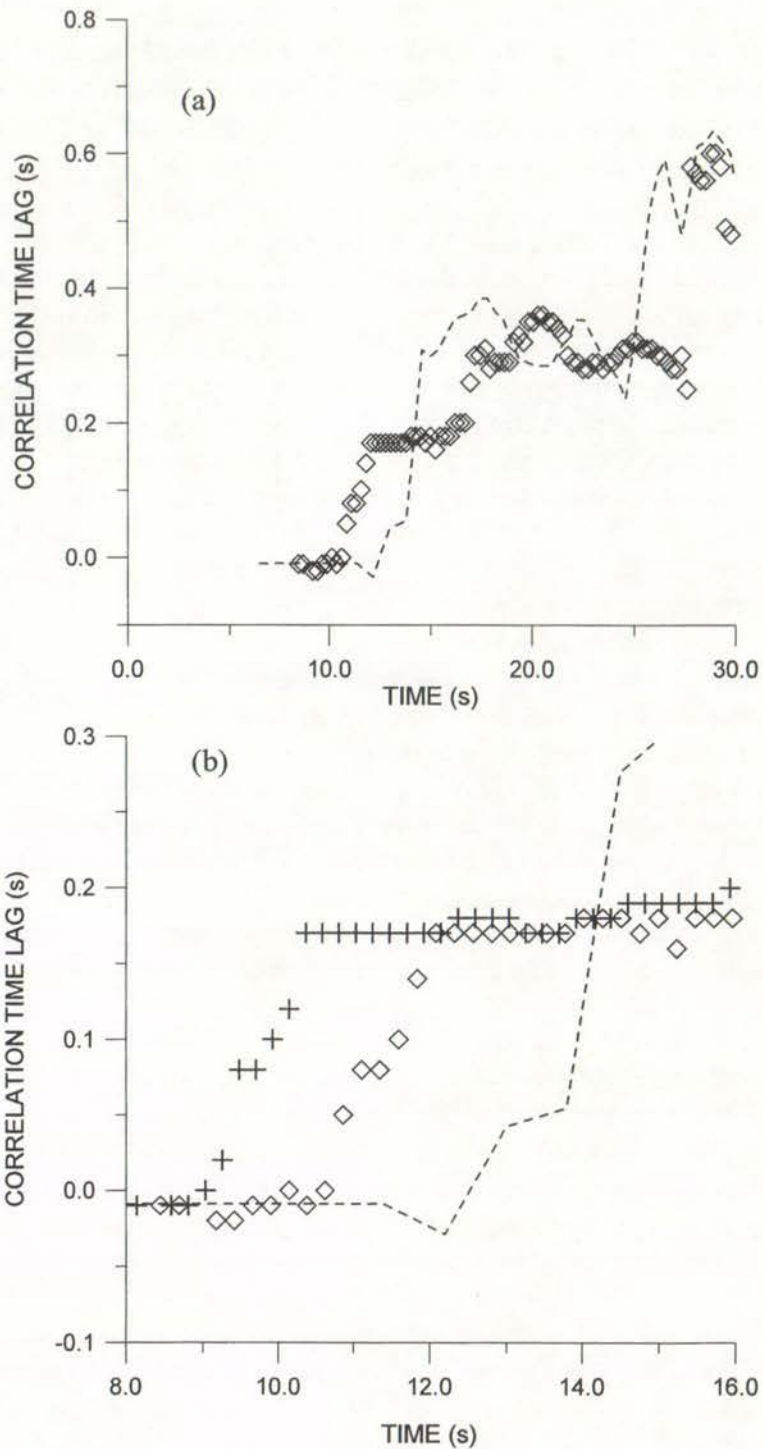


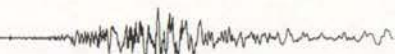
Figure 13. Comparison of time compression (dashed line) and individual window correlation results. (a) Result for 6.4 s window. (b) Comparison of 6.4 s result (\diamond) with that for 9.6 s window (+).

associated with correlations for a window of 6.4s duration moving across the entire record. Each of the data points results from correlating the two acceleration records over the time window and then plotting the lag versus the time at the centre of the window. If one halves the window size to 3.2 s, the results become erratic and many points plot well off the scale of the graph. In order to compare the 6.4s results with the time compression method, we have biased the data in the figure downward by



0.7s. This accounts for the time compression results being the *additional* lag time over and above the lag associated with small deformation elastic waves. The time compression result for the interval $(t_F - t_S)$ of 0.4 s is shown by the dashed line on the figure. There are similarities between the two data sets but there are significant differences in the timing of the major softening jumps. We can easily discover the root cause of the differences by performing a second individual correlation calculation using a greater window duration. Results are shown on an enlarged time scale in Figure 13b. The diamond shaped data points are identical to those shown in Figure 13a for the 6.4s window. The + data points correspond to the second calculation using a window width of 9.6s. The dashed line shows the time compression result. The striking point about this figure is the similar shape but different timing exhibited by the two individual window results. The 9.6s window data show the first strong softening occurring between 9.4 and 10.5s. The same effect does not appear for the 6.4s window until roughly 10.7s, and it ends at about 12s. The reason for this becomes clear when one inspects the original acceleration records. Referring to Figure 3, note the ground surface acceleration peaks marked *A* and *B*. These occur at roughly 14.0s and 15.1s. The 6.4s window will just begin to encompass peak *A* when the centre of the window lies at $14.0s - 3.2s = 10.8s$. It will encompass peak *B* when its centre lies at $15.1s - 3.2s = 11.9s$. These times almost exactly coincide with the times for the softening indicated by the diamond shaped points on Figure 13b. The longer window duration of 9.6s encounters the peaks somewhat earlier. The exact time difference will be $4.8s - 3.2s = 1.2s$, and this is nearly exactly the time separating the two correlation results. It is evident that using individual time windows in this way may lead to flawed understanding. The lag time is dominated by the major peaks of the acceleration record, to the extent that the correlation result is instantaneously skewed as soon as the peak enters the window.

Next we consider the North-South component for the 0 and 16 m depth instruments. The 12 s – 20 s segment of the North-South acceleration record is illustrated in Figure 14. As before, visual inspection suggests the records are correlated although the correlation is not as clear cut as in Figure 3. If we carry out the time compression algorithm here, the before and after correlation graphs are found in Figure 15. Before time compression the peak correlation lag was 0.37 s. After time compression it is reduced to 0.08 s, slightly larger than the value of 0.07 s found for the East-West records. The cumulative time compression is also somewhat different in this case. It is shown in Figure 16. The East-West cumulative compression from Figure 9 is shown there also as a dashed line. Both results were obtained using the $(t_F - t_S)$ interval of 0.8 s. It is evident from Figure 16 both the North-South and East-West records are in broad agreement. Both suffer dramatic time compression around 14 seconds and both have a final cumulative compression value near 0.3 s. However, the North-South record does not reveal the dramatic increase and decrease in time compression found between 25 s and 35 s on the East-West record. Realising that the cumulative time compression is inversely proportional to the shear modulus, the differences in time compression may suggest anisotropic effects may be present. However, they are of a transient nature, and the soil appears to be more or less isotropic at the conclusion of shaking. This is consistent with the surmise that much of the softening results from increased pore pressure and liquefaction effects.



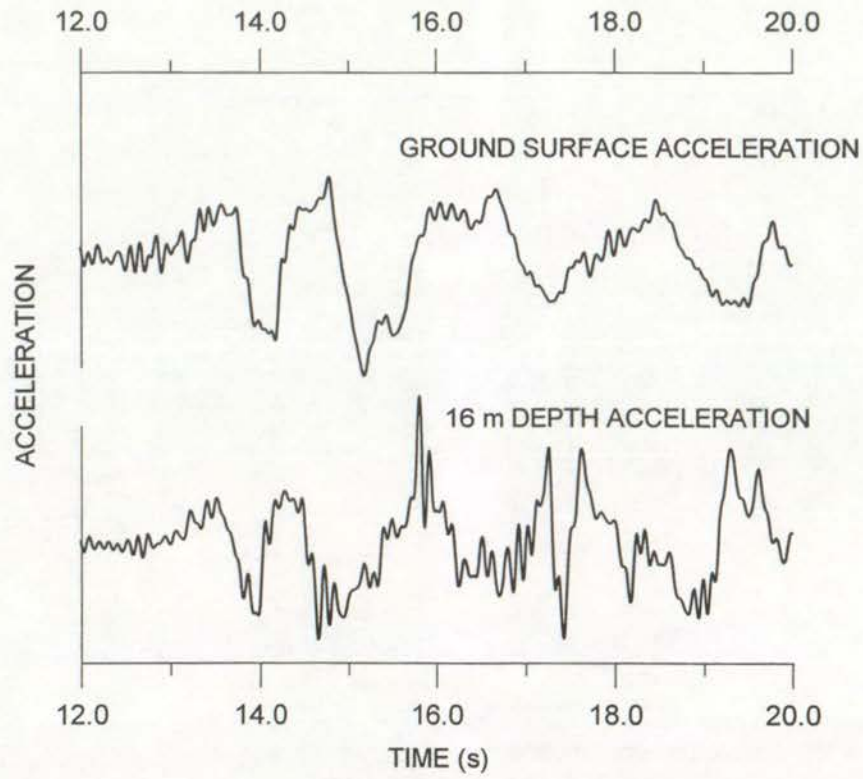


Figure 14. Part of the North-South Port Island acceleration records from 0 and 16 m.

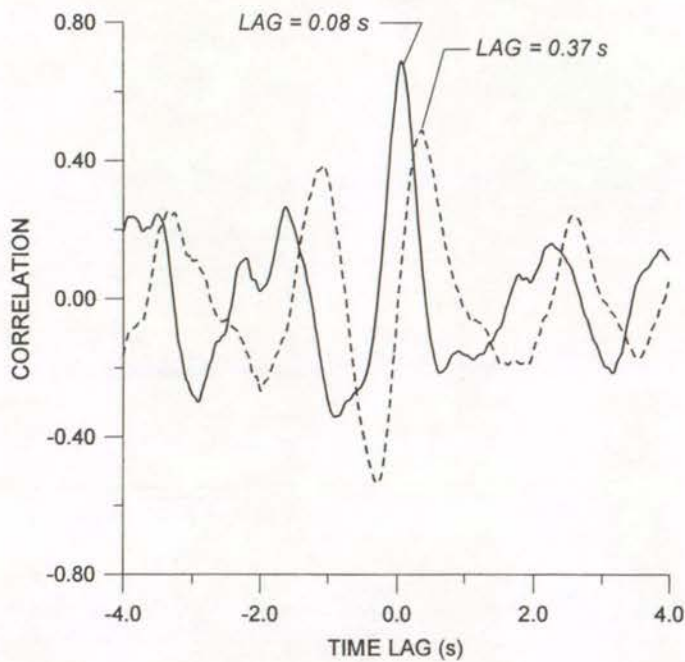
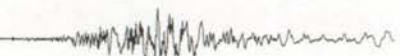


Figure 15. Correlation of Port Island North-South data from 0 and 16 m: dashed line shows correlation of original data; solid line shows correlation after time compression.



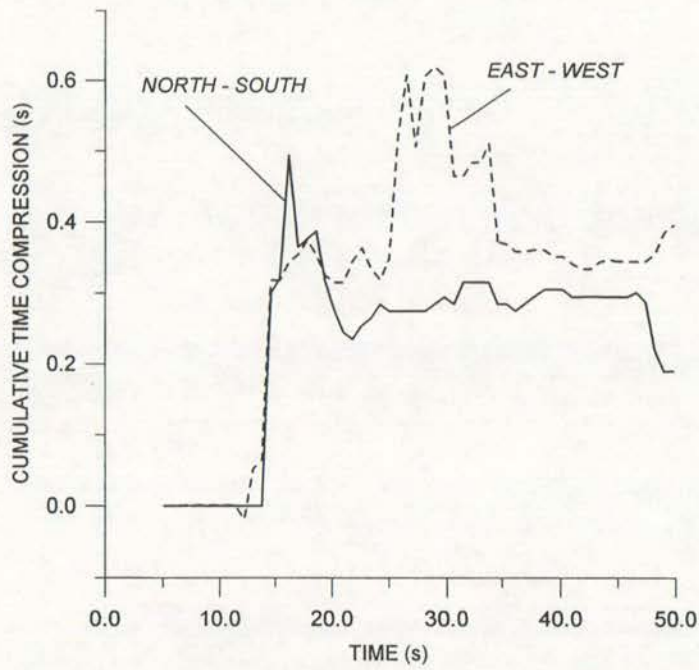


Figure 16. Cumulative time compression curves compared: solid line for North-South data, dashed line for East-West data.

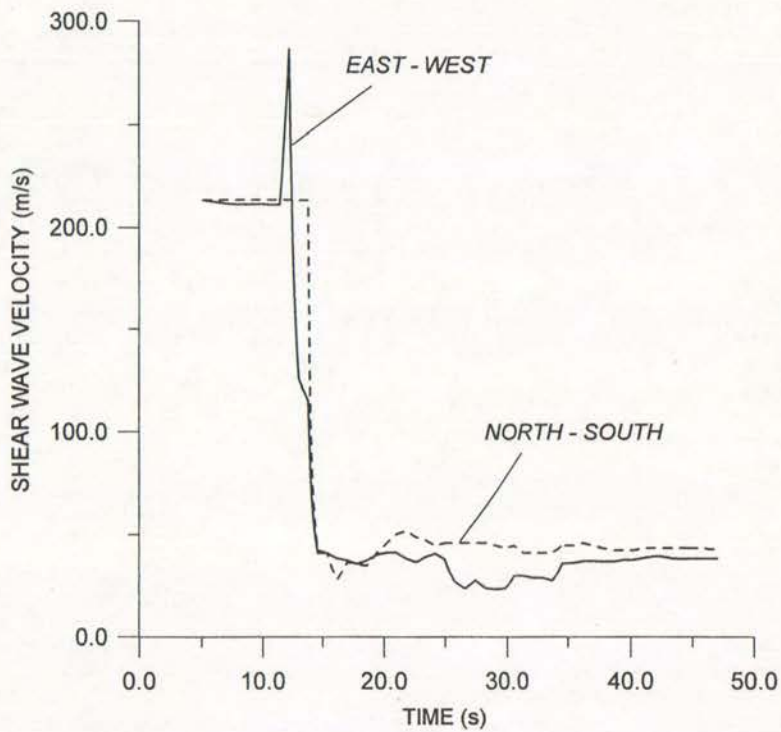
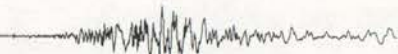


Figure 17. Estimated average shear wave velocity between 0 and 16 m depth at Port Island. Solid line for East-West data, dashed line for North-South.



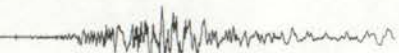
Note that the North-South and East-West records give different estimates for the small deformation elastic lag time. The average of the two values is 0.075 s . Using this average value for t_0 , two curves for shear wave velocity based on equation (7) are shown in Figure 17. The solid line refers to the East-West data, the dashed line to the North-South data. Note the relatively muted effect of the transient jump in time compression between 25 and 35 s on the East-West record. The peculiar spike in the East-West response at about 12 s is caused by the slight time stretching that occurs at that time in Figure 9a. This time stretching is not thought to be representative, but it does have a dramatic effect on the shear wave velocity calculation as can be seen from equation (7). With t_0 equal to 0.075 s , the negative value for C_m equal to -0.019 s results in a shear wave velocity of 286 m/s . This is not considered realistic. We can offer no explanation for the time stretching at 11 s, but it seems highly unlikely stiffening would occur at this point in the record.

Finally we note that seismic profiling was carried out at the Kobe site to estimate the small deformation shear wave velocity structure. As reported by Iwasaki and Tai [2], the uppermost 5 m soil segment was assigned a velocity of 170 m/s while in the segment between 5 m and 19 m the shear wave velocity was found to be 210 m/s . This suggests a small deformation shear wave velocity for the 0 m – 16 m depth of 198 m/s . This value is close to the initial shear wave velocity of $16\text{ m}/0.075\text{ s} = 213\text{ m/s}$ obtained from the average of the time compression results for the East-West and North-South records.

Elmore Ranch

In November 1987, two earthquakes occurred near a site in the Imperial Valley, California, where extensive field instrumentation had been placed by the US Geological Survey [14,15]. The site was part of a wildlife refuge and has come to be called the Wildlife Site, or simply Wildlife. The Wildlife Site became of interest following the Westmorland earthquake in 1981. That earthquake appeared to have caused liquefaction in certain areas, Wildlife being one. The site was subsequently instrumented to study the effects of liquefaction. Two accelerometers were placed at the site, one at 7.5 m depth below ground surface and one at ground surface; as well as six piezometers at depths ranging between 2.9 m and 12.0 m. Site stratigraphy is illustrated in Figure 18. A layer of silt approximately 2.5 m thick overlies a 4.5 m thick layer of silty sand. The water table is located at a depth of about 1.2 m. The silty sand was presumed to be liquefiable. It lay above a 5 m thick layer of stiff clay. The downhole accelerometer was positioned near the upper surface of the stiff clay.

In November 1987, two earthquakes occurred near Wildlife within a period of 12 hours. The first was the Elmore Ranch earthquake. It had magnitude 6.2 and was located approximately 23 km west from Wildlife. The second was the Superstition Hills earthquake: magnitude 6.6, located approximately 31 km to the west and south from Wildlife. At the ground surface the peak measured acceleration for the Elmore Ranch event was 0.13 g , and for the Superstition Hills event, 0.21 g . Three



component acceleration records for both events were obtained from both the surface and the downhole instruments.

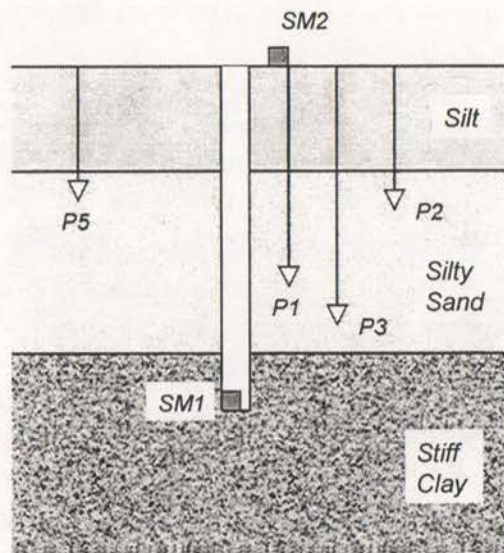


Figure 18. Schematic soil profile at Wildlife. Downhole and Surface accelerometers denoted by square boxes SM1 and SM2. Piezometers are denoted by triangles P1, P2, P3 and P5.

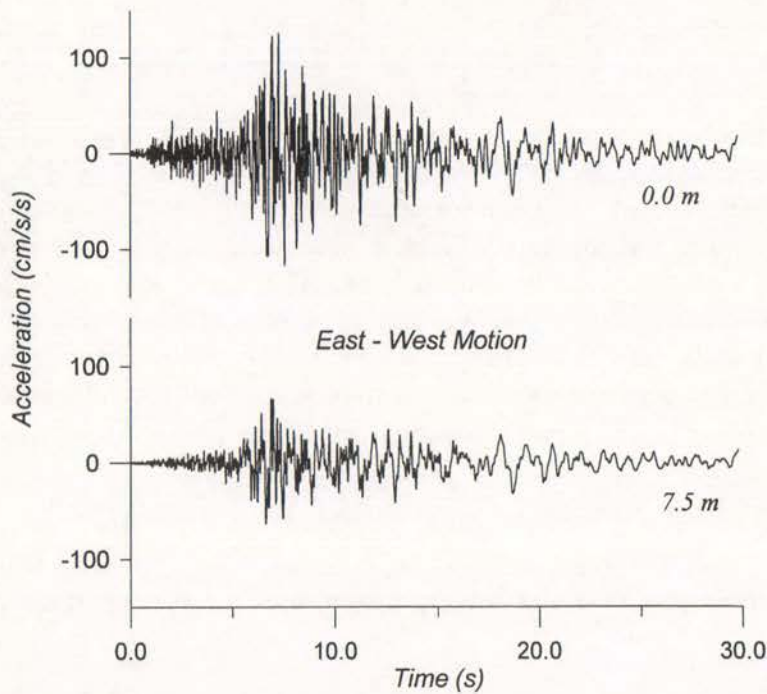


Figure 19a. Measured accelerations for Elmore Ranch: East-West component.



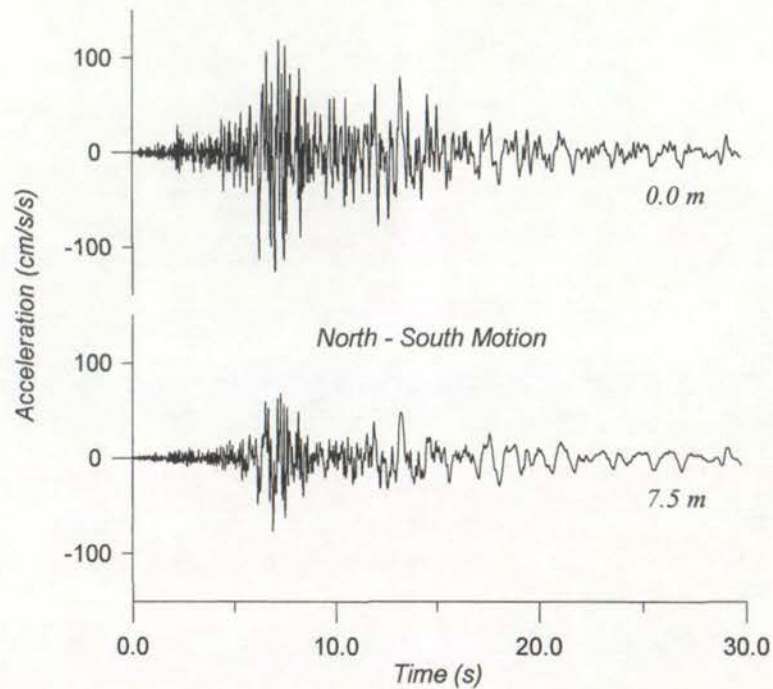
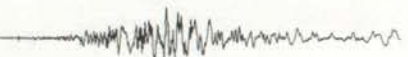


Figure 19b. Measured accelerations for Elmore Ranch: North-South component.

Figure 19 shows the horizontal acceleration records for the Elmore Ranch earthquake. For the Elmore Ranch event the peak ground surface acceleration of slightly less than $0.13g$ was found in both the North-South and East-West records. It occurred in both records at about 7 seconds. The duration of strong shaking (accelerations exceeding $0.05g$) was slightly less than 10 seconds for the North-South record and about 7 seconds for the East-West record. The field piezometers in the Wildlife array recorded no excess pore pressure development during this earthquake. It seems unlikely any significant softening occurred. Correlation of the unaltered records would therefore be expected to provide a good estimate for the small deformation shear modulus for the site. Figure 20 shows the correlation of the North-South data. Correlation of the East-West records gives a similar picture.

Figure 20 clearly shows two correlation peaks, one at $0.070s$ corresponding to the direct or upward traveling waves, and one at $-0.065s$ corresponding to reflected or downward traveling waves. These two figures compare favorably with the value of $0.060s$ quoted by Holtzer, *et al.*, [14] as the elastic wave travel time for the upper $7.5m$ at the Wildlife site.

Next we can apply the time compression algorithm to the Elmore Ranch data. One would clearly expect to find little or no time compression, indicative of there being no softening caused by this earthquake. In fact, this is not the actual result, as shown in Figure 21. On the figure, both the North-South data (solid line) and East-West data (dashed line) cumulative time compression results are shown. Both graphs were obtained using a single pass with $(t_F - t_S)$ equal to 1.6 seconds. While the results for both directions agree with each other, they are clearly counter-intuitive. A small amount of time compression occurs in the first 7 to 8 seconds, but significant *time stretching* then follows. This would appear to indicate stiffening of the Wildlife soils.



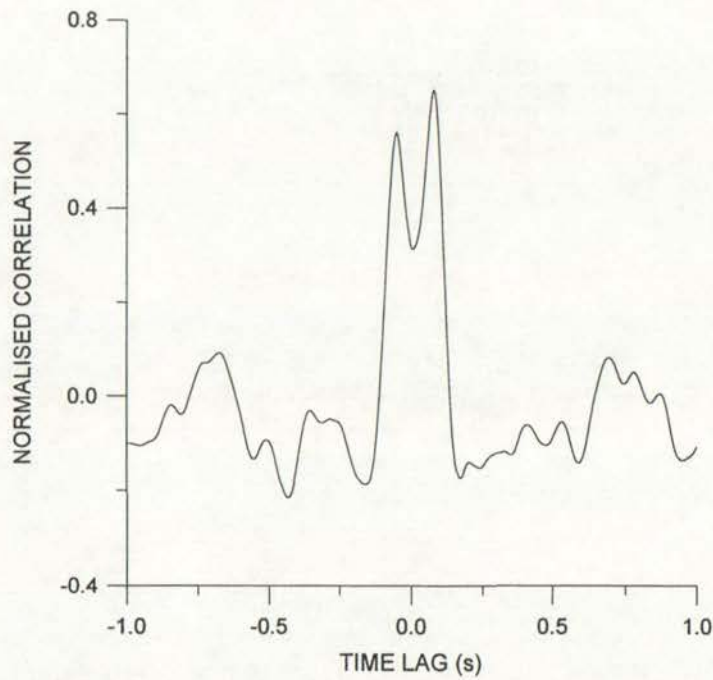


Figure 20. Normalised correlation for North-South Elmore Ranch data.

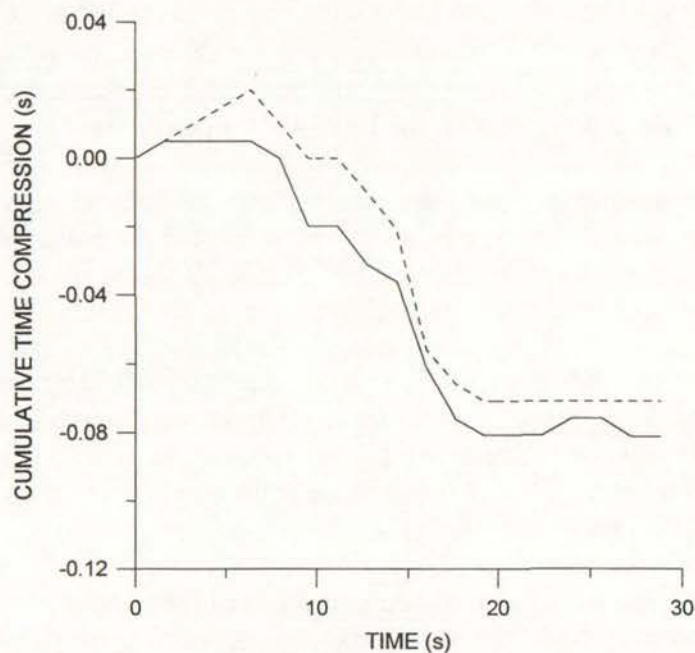
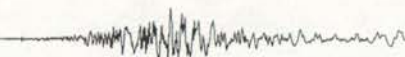


Figure 21. Cumulative time compression for Elmore Ranch. Solid line for North-South data, dashed line for East-West data.

In fact it is highly unlikely the Wildlife site stiffened during the Elmore Ranch event, especially by the amount suggested in Figure 21. It seems clear the apparent stiffening is fictitious and therefore we can speculate about its origin. The most likely explanation appears to be surface waves. Our time compression algorithm (and any correlation-based technique for that matter) assumes the ground motion



results from vertically propagating SH waves. If in fact surface waves are the predominant form of ground motion, then little vertical propagation is occurring and the apparent travel time between the downhole and surface instruments is zero. In the case of the North-South data, the lag time associated with the final correlation for time compression suggested an elastic wave travel time of 0.08 seconds. This is precisely the negative of the amount of time stretching found at the end of the record (see Figure 21). For the East-West data the corresponding figure was 0.07 seconds, also exactly equal to the final amount of time stretching. This strongly suggests that at later stages of the record the algorithm recognised an apparent zero travel time for waves, exactly what would have happened if surface waves were the predominant wave form.

Our surface wave explanation must remain speculative since no precise determination of the wave form can be made. Nevertheless, the suggestion does appear reasonable. It is further supported if one carries out a series of correlations over individual time windows, as was done in Figure 13a for example. Figure 22 illustrates the result for the North-South data. The time compression result from Figure 21 is also shown for comparison. In the figure the individual window data has been reduced by 0.07 seconds, the apparent elastic wave travel time. The window size was 3.2 seconds. It is evident the individual window result is basically the same as for time compression.

The Elmore Ranch event, although appearing quite innocent, presents a difficult test for the time compression algorithm. This is evident from the basic results in Figure 21, but is even more clear if we attempt to reduce the time interval ($t_F - t_S$). An interval of 1.6 seconds was used for Figure 21. If we repeat the time compression while halving the interval to 0.8 seconds, we find the results shown in Figure 23.

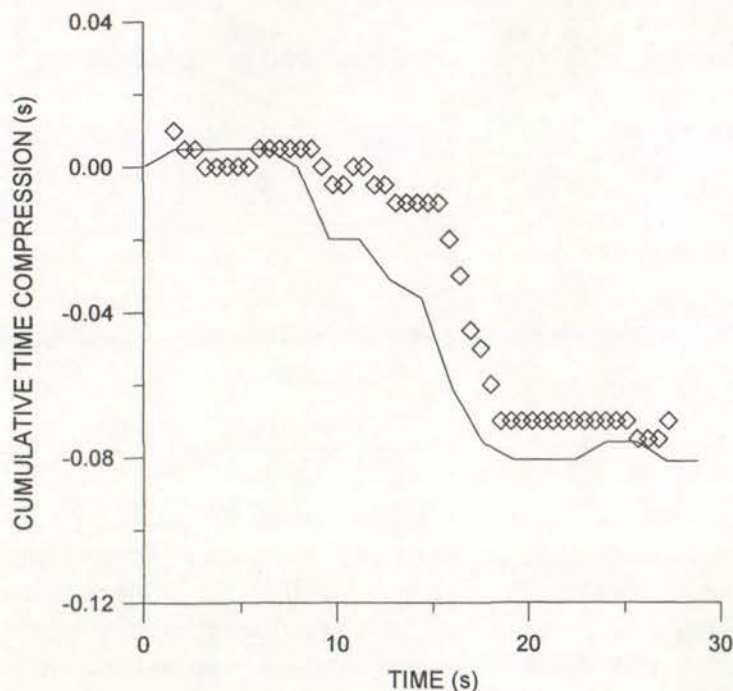
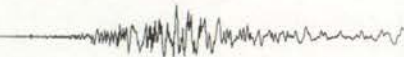


Figure 22. Cumulative time compression for North-South Elmore Ranch data. Time compression algorithm: solid line; individual window correlation: \diamond .



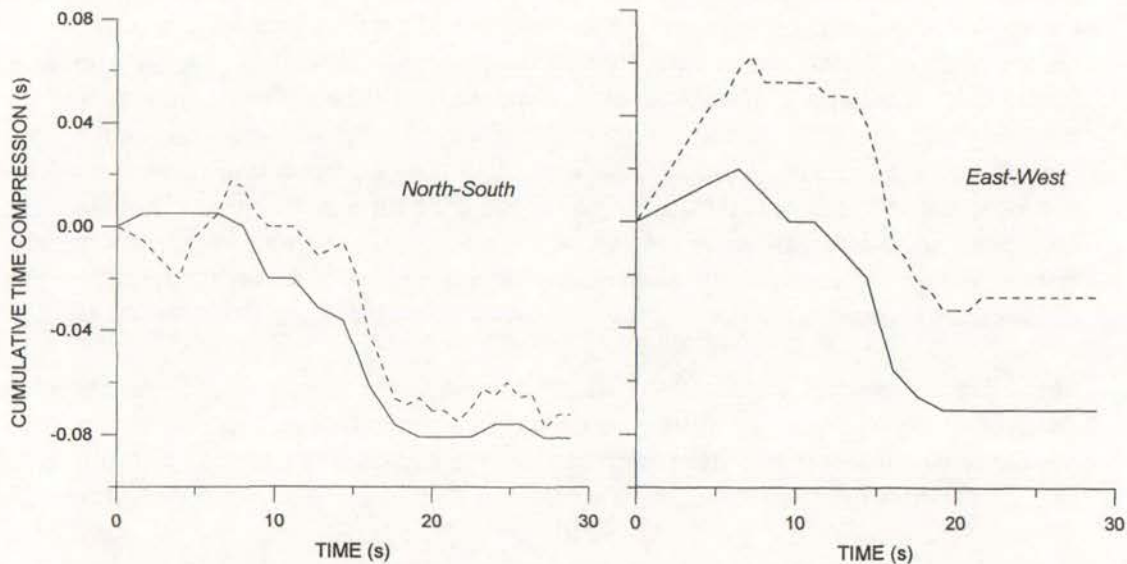
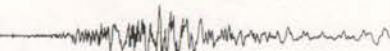


Figure 23. Graphs of cumulative time compression for Elmore Ranch. Effect of re-running the algorithm with halved time step. Solid lines are same as Figure 21. Dashed lines are for halved time interval.

In Figure 23 both the original results for $(t_F - t_S)$ equal to 1.6 seconds and the recalculated result for $(t_F - t_S)$ equal to 0.8 seconds are shown. For the North-South record, the repeated calculation is somewhat more erratic or jagged than the original, but the trends are essentially the same. This is the expected result. For the East-West data, however, the repeated calculation gives a significantly different result from the original. The new cumulative time compression suggests more softening occurred early in the record and less time stretching later. This is unexpected and cannot be considered realistic. Evidently the initial compression with $(t_F - t_S)$ equal to 1.6 seconds introduced a spurious phase shift that the second compression attempts to correct. This example makes clear the importance of using larger intervals $(t_F - t_S)$ as discussed earlier in the report. It also emphasises the delicate nature of the algorithm itself. Care is needed here as in any application of multi-variate optimisation and all results must be judged carefully for a reasonable outcome.

Superstition Hills

The Superstition Hills earthquake occurred only 12 hours after the Elmore Ranch earthquake. Its magnitude was 6.6, slightly larger than the Elmore Ranch value of 6.2. Both surface and downhole instruments at Wildlife recorded complete records. In addition, all but one of the piezometers recorded pore pressure increases. It appears that liquefaction occurred in the silty sand layer between depths 2.5m and 7.0m. This hypothesis is supported both by the measured pore pressures and by surface features such as sand boils and evidence of lateral spreading. Plots of surface and downhole horizontal accelerations are shown in Figure 24.



The peak horizontal acceleration at the ground surface was 0.21g in the North-South direction at about 13.6 seconds after the array triggered. At the 7.5m depth the peak acceleration was about 0.17g, also in the North-South direction and at the same time. Even a cursory inspection of the records suggests that significant softening occurred following the peak response. At the ground surface a lower predominant frequency is evident, as are characteristic acceleration spikes separated by more or less flat response. These acceleration spikes have been implicated in a number of earthquakes as evidence of softening, probably due to liquefaction [16].

We will begin by working through the East-West record in some detail. Correlation of the original acceleration records produces the dashed line shown on Figure 25. It is clear from the shape of this line that the surface and down hole records are not well correlated. The peak correlation is little greater than several other nearby maxima. Its normalised magnitude is only 0.212. It lies at a lag time of 0.10 seconds. Use of the time compression algorithm enhances the correlation considerably. A single pass with $(t_F - t_S)$ equal to 1.6 seconds produces the solid line shown on Figure 25. The peak correlation now has a magnitude of 0.466. It is significantly emphasised in comparison with the surrounding peaks. However, the lag time associated with this peak is now exactly zero. Obviously this cannot be considered an acceptable approximation for the elastic wave travel time between the instruments. If we now re-use the algorithm on the adjusted data with $(t_F - t_S)$ equal to 0.8 seconds, the peak correlation is again raised significantly and becomes 0.543. The associated lag time is now 0.11 seconds. Evidently time compression is effective at improving the correlation, but the estimates for the elastic wave travel time are erratic.

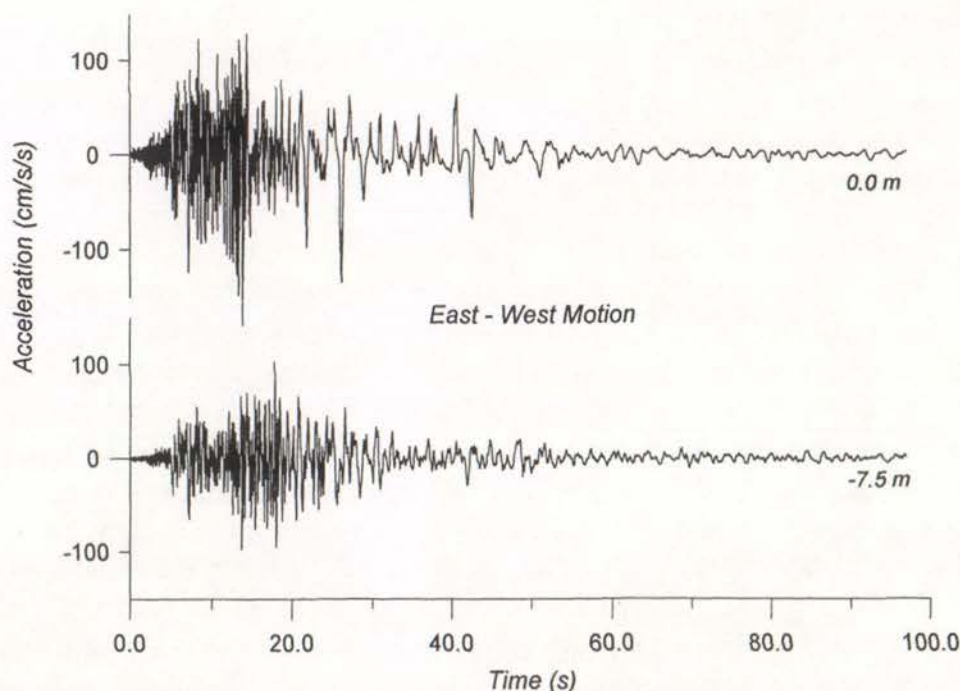
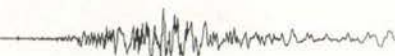


Figure 24a. Measured accelerations for Superstition Hills: East-West component.



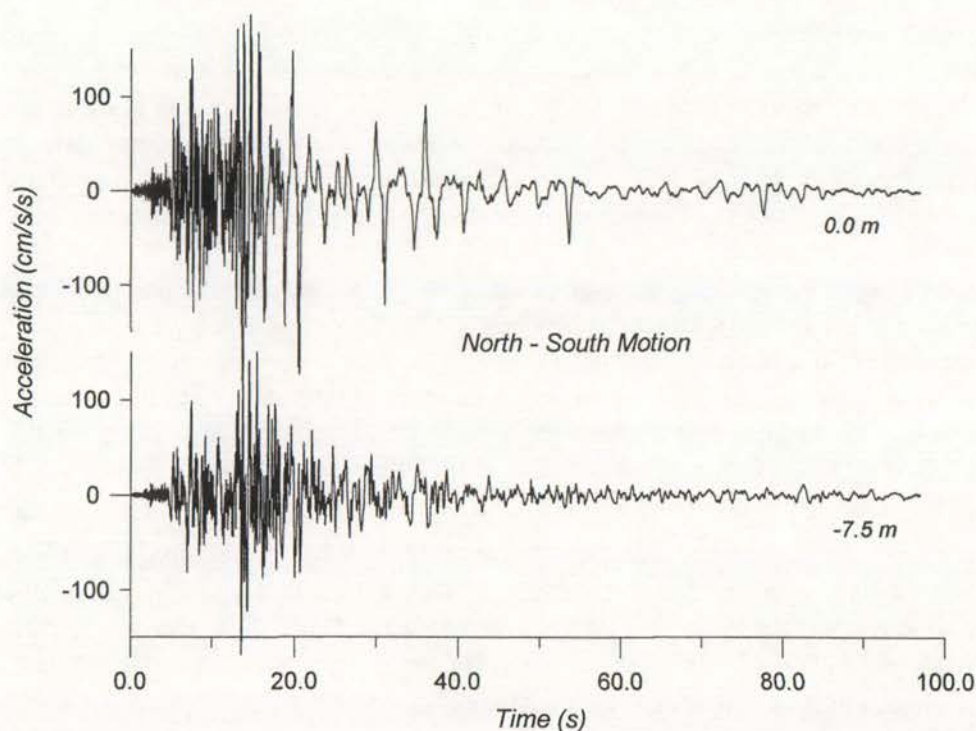


Figure 24b. Measured accelerations from Superstition Hills: North-South component

The graphs of cumulative time compression for both values of $(t_F - t_S)$ are shown in Figure 26. The result for $(t_F - t_S)$ equal to 1.6 seconds is shown by the thin solid line. The result for $(t_F - t_S)$ equal to 0.8 seconds is shown by the dashed line. The sum of the two results is given by the heavy solid line. Note how the dashed line does not hover around zero as one might expect. Instead it takes on consistently negative values over most of the full 100 seconds of the record.

The cumulative time compression behaviour shown in Figure 26 is particularly interesting. The initial pass, using $(t_F - t_S)$ equal to 1.6 seconds, produced significant compression early in the record, prior to the peak ground acceleration at 13.6 seconds. Other researchers [3, 14, 15] have asserted that either no softening, or possibly very little softening, occurred at Wildlife prior to the time of the peak acceleration. With $(t_F - t_S)$ equal to 1.6 seconds, the cumulative time compression reached a value of 0.11 seconds prior to the peak acceleration. This would suggest the wave travel time had at least doubled by this point in the earthquake, a result that seems highly unlikely. The effect of the second pass through the record, using $(t_F - t_S)$ equal to 0.8 seconds, almost completely removes the compression found in the first attempt. Note how the heavy solid line in Figure 26 remains near zero up to the time of the peak acceleration. Once the 13.6-second threshold is passed, the second time compression then proceeds more or less as one would expect, showing only small changes to the original result. Thus the consistently negative



aspect for the 0.8 second result seems much more sensible in light of the difficulty experienced by the 1.6 second compression in the early parts of the record.

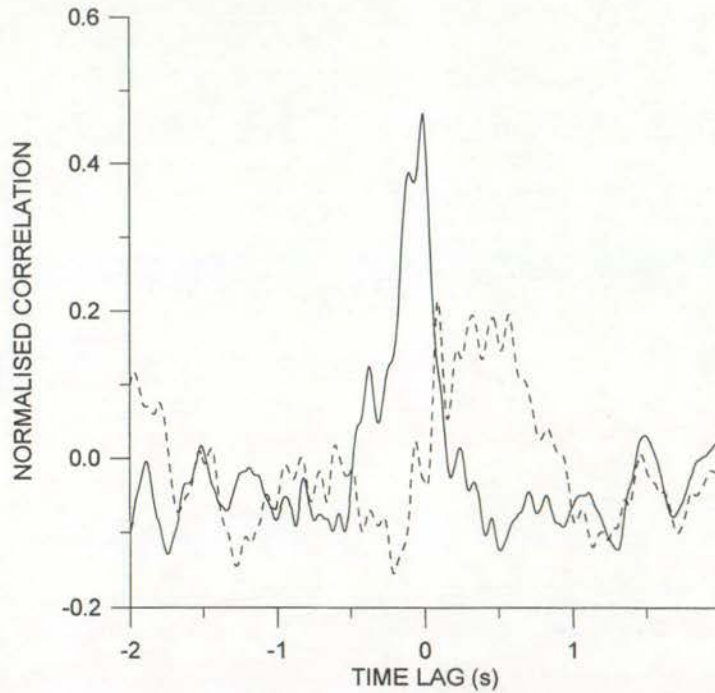


Figure 25. Correlations for East-West Superstition Hills data. Dashed line before time compression, solid line after.

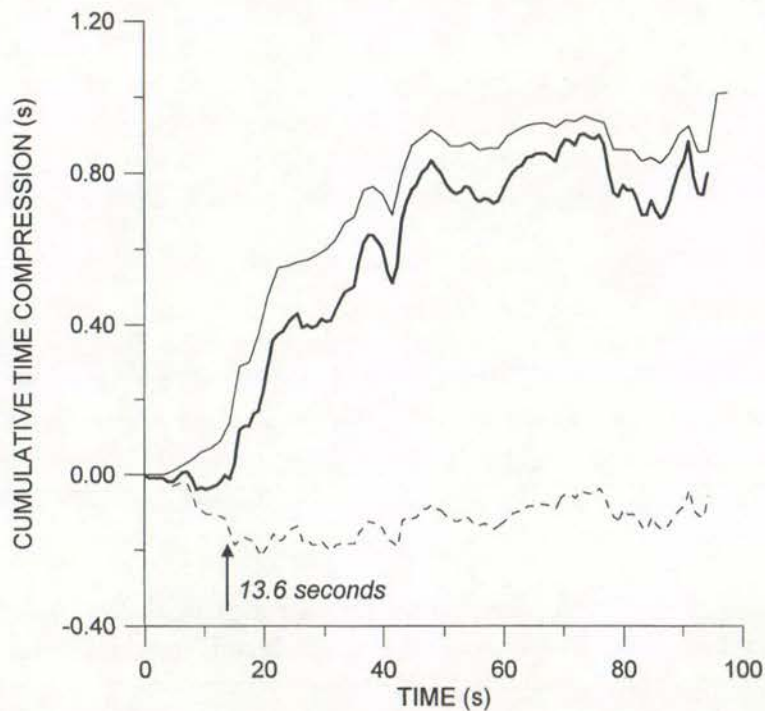


Figure 26. Cumulative time compression for East-West Superstition Hills data. Heavy solid line is the sum of the light line (1.6 second interval) plus the dashed line (0.8 second interval).



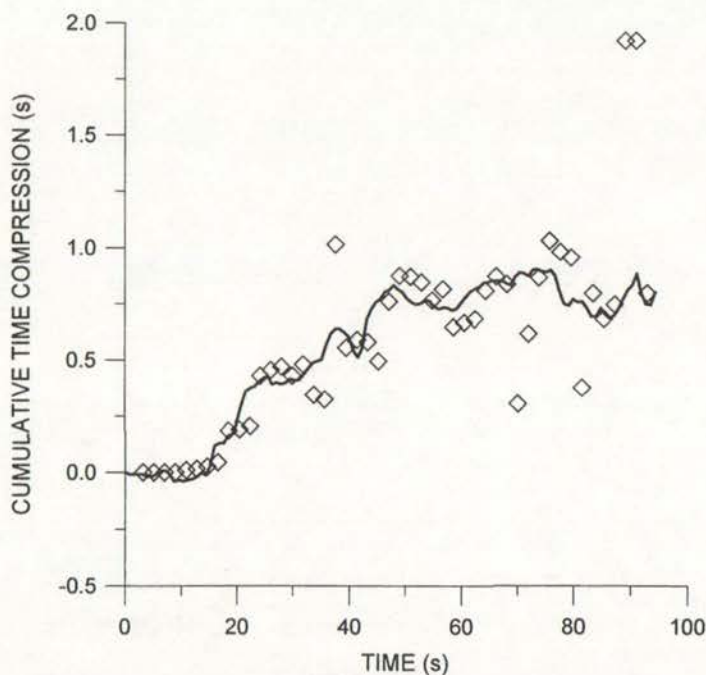
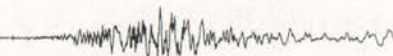


Figure 27. Comparison of cumulative time compression results for Superstition Hills East-West data. The solid line is the same as Figure 26. The symbols \diamond result from correlation over individual windows.

We can also attempt to analyse the record using individual window correlations. The result for windows of 6.4 second duration is shown in Figure 27. For comparison the result after the 0.8-second compression is also shown. Evidently, the individual window correlations are slightly erratic, particularly for the latter stages of the earthquake. The time compression algorithm appears to produce a more useful result for these records.

Turning attention to the North-South records, note from Figure 24 that the North-South accelerations were slightly stronger than the East-West. The peak acceleration occurred in the North-South direction and the transition from high frequency to low frequency motion following the peak is somewhat more distinct than for the East-West record. Figure 28 shows the normalised correlations for the North-South record before and after the initial time compression using $(t_F - t_S)$ equal to 1.6 seconds.

Comparing Figures 25 and 28, we see that the initial correlation of the North-South data suggests the downhole and surface records are better correlated than for the East-West record. The peak correlation for the original North-South data is 0.434 at a lag time of 0.09 seconds. Following the initial time compression the peak correlation is increased to 0.586. The lag time is reduced even more than in the case of the East-West data to a value of -0.01 seconds. It is not clear why the lag associated with the first time compression for both the East-West and North-South records is so drastically reduced. A second application of the time compression



algorithm using $(t_F - t_S)$ equal to 0.8 seconds further increases the peak correlation to 0.610 and changes the lag time to 0.04 seconds.

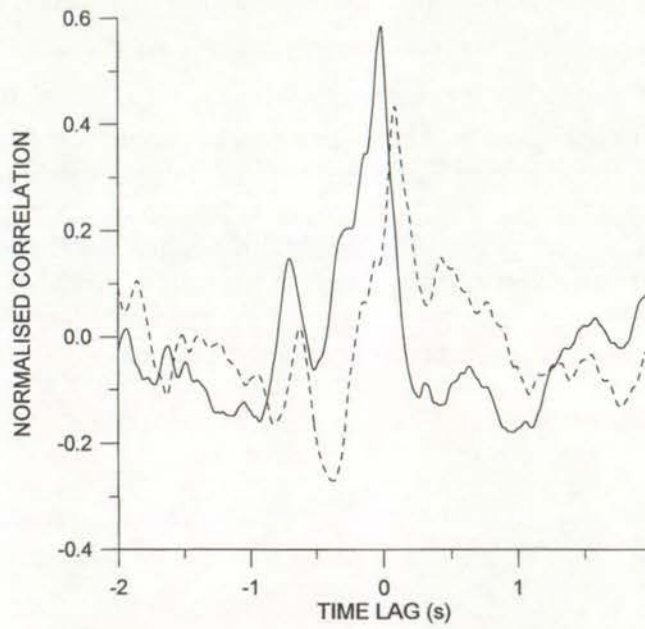


Figure 28. Correlations for North-South Superstition Hills data. Dashed line before time compression, solid line after.

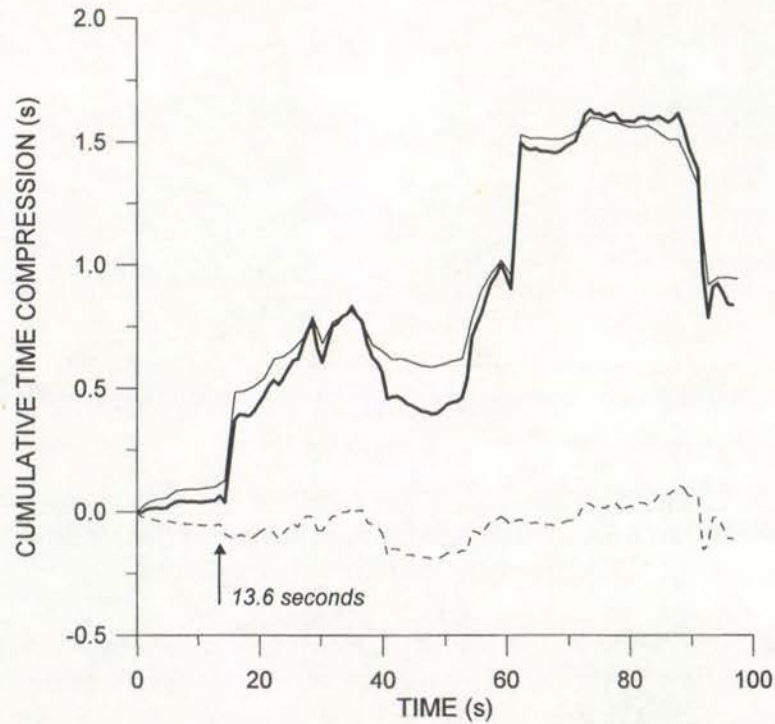


Figure 29. Cumulative time compression for North-South Superstition Hills data. Heavy solid line is the sum of the light line (1.6 second interval) plus the dashed line (0.8 second interval).



Graphs of cumulative time compression of the North-South Superstition Hills data for $(t_F - t_S)$ of 1.6 and 0.8 seconds are shown in Figure 29. The result for $(t_F - t_S)$ equal to 1.6 seconds is represented by the thin solid line. The dashed line shows the effect of re-running the algorithm with $(t_F - t_S)$ equal to 0.8 seconds, while the heavy solid line gives the composite result for both compressions. These results are similar to those for the East-West data in that the first time compression suggests softening prior to 13.6 seconds while the second compression evidently attempts to correct that impression. The North-South results are significantly different from the East-West results later in the earthquake, however. The difference can be seen more clearly on Figure 30 where the composite cumulative time compressions after the second application of the algorithm for both sets of records are shown.

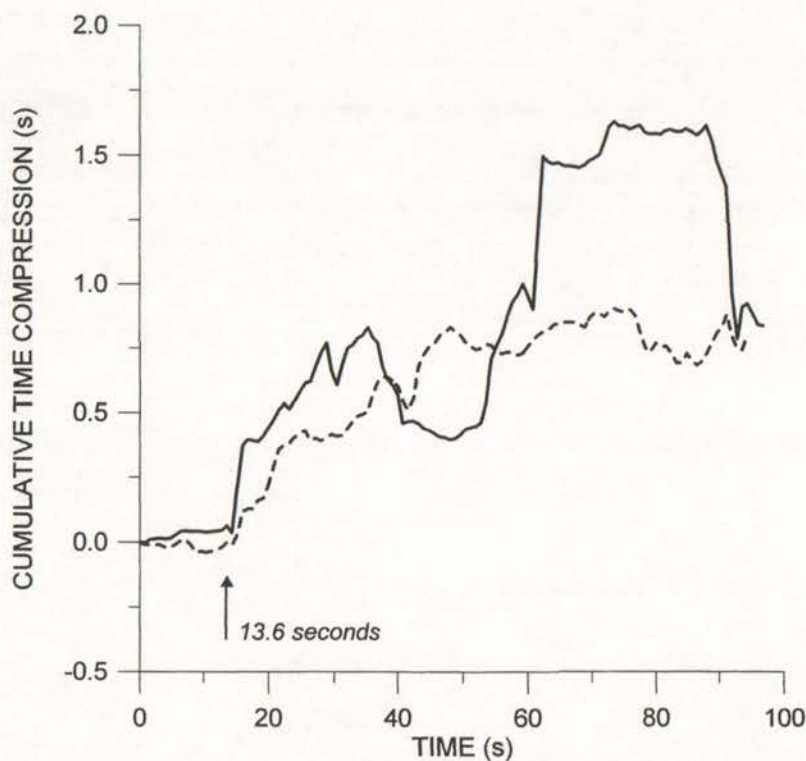


Figure 30. Comparison of cumulative time compression results for North-South (solid line) and East-West (dashed line) acceleration data from Superstition Hills earthquake

It is evident from Figure 30 that while the time compression results for the two sets of data are similar over the initial 40 seconds of the earthquake, there are substantial differences later, particularly between 65 and 95 seconds. Over that time interval the North-South cumulative time compression is roughly double that for the East-West. Note however, that both results suggest very large amounts of softening have occurred. If we convert the time compression values into corresponding shear wave velocities, the differences become much less dramatic. For the 65 – 95 second time



interval the average shear wave velocities for the North-South and East-West results are roughly 4.5 m/s and 8.6 m/s respectively. When these figures are compared to the original wave speed of about 125 m/s the difference is clearly not appreciable.

Finally we can compare the time compression result for the North-South data with the corresponding individual window correlations. This is done in Figure 31. The window duration was 6.4 seconds. The result for individual windows is evidently inferior to that for time compression.

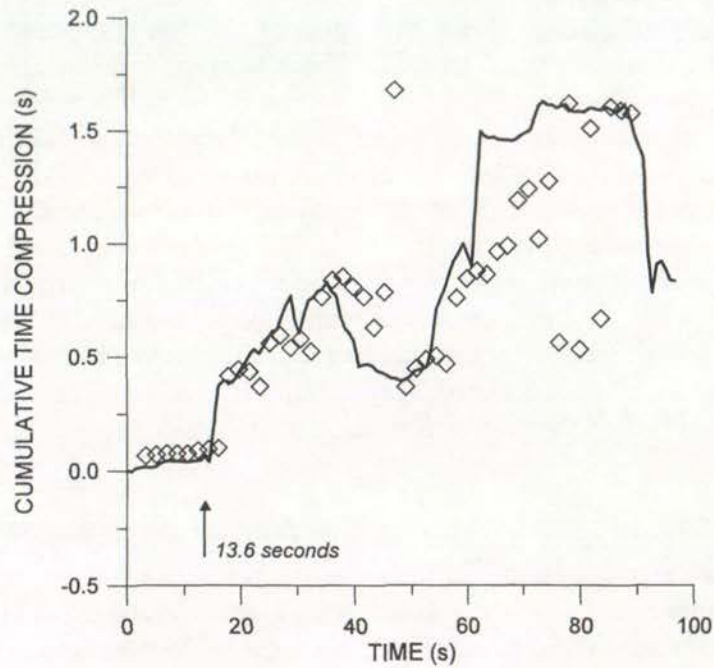


Figure 31. Comparison of cumulative time compression results for Superstition Hills North-South data. The solid line is the same as Figure 29. The symbols \diamond result from correlation over individual windows.



SUMMARY AND RECOMMENDATIONS FOR FUTURE WORK

The time compression algorithm presented here possesses several advantages for estimation of shear modulus or shear wave velocity from downhole acceleration records. First, the algorithm is an extension of the time-honoured method of correlation used for weak ground motion. There is no need to resort to elaborate modeling, only the surface and downhole acceleration records are needed. Second, the algorithm is physically appealing. The idea of time compression bringing the upper acceleration record into closer correlation with the lower is easily grasped and acted on. The algorithm is also computationally straightforward and efficient. For both the East-West and North-South Port Island records discussed above, the complete calculation time on a 133 MHz Pentium PC did not exceed 150 seconds. The Superstition Hills data files are considerably longer but they still required less than five minutes to process. Another advantage is the ability of the algorithm to be used repetitively. If one questions the result of the first time compression computation, a second application will quickly show whether the initial result was acceptable or not.

On the other hand, numerical solutions of optimisation problems such as this one are usually delicate calculations. In the present case we have a large multivariate problem, the dimension of the optimisation being equal to M , the number of time intervals for compression. Fortunately it is not required to *simultaneously* optimise all the Δ_m 's; nevertheless the 'lumpy mattress' effect may still exist for this problem and it may create difficulties in some circumstances. For example, one can envision a pathological situation in which the calculated time compression Δ_m is greater than the segment size. This would imply time is inverted in the segment, not a possibility that could be entertained in any circumstances. Fortunately the algorithm developed here appears to be reasonably robust in this regard. The Superstition Hills records clearly present a severe test, yet the calculations shown above were performed without excessive care and the results for softening appear to be consistent and sensible even though the elastic travel time estimates were erratic.

In many ways the Elmore Ranch data present the greatest difficulty for the algorithm. Even if we disregard the apparent surface wave effects in the later parts of the records, it is evident that the results given by time compression are less than ideal. This is particularly true for the East-West data. In that case the repeated use of the time compression algorithm completely failed to produce realistic results. It seems likely the first compression introduced changes within the record that suggested softening occurred, when in fact it had not. The Elmore Ranch data are characterised by high frequency excitation across early parts of the record but lower frequency motion in later parts, presumably due to surface waves. In the high frequency region, even small amounts of time compression may shift peaks and troughs in such a way as to make it appear some softening may have occurred. The change to lower frequencies may suggest softening as well.



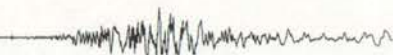
Returning to the positive attributes of the algorithm, the comparison between time compression results with results from segmental correlation over individual windows shows clearly that time compression gives a more accurate picture of the way in which softening occurred. The two methods give generally similar results, but the use of individual windows appears to be strongly influenced by the window duration and to produce occasional stray results that have little relation to the results from other windows.

While the time compression algorithm appears to have considerable promise, there are aspects that might be improved with further work. The use of uniform sized time intervals is restrictive and probably inefficient. It seems reasonable that larger time intervals might be used in parts of the record where little softening is occurring, and smaller intervals used over periods of stronger motion. The point that is not yet clear is how to predetermine which parts of a record are strong (in the sense that softening is occurring) and which are not. There is also a need for a mechanism within the computer code to prevent the optimisation scheme jumping to a fallacious correlation peak. This appears to be the cause of sudden shifts in the predicted lag time (or elastic travel time) that are unexplained by softening. The 'lumpy mattress' will always be present in a multivariate problem such as this, but there may be a strategy for helping the computation to adhere to the correct peak. Finally, there will be opportunities in the future to test the algorithm on other downhole records as they become available.

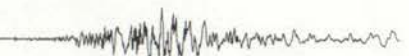


References

1. Ishihara, K., Muroi, T., and Towhata, I., 'In-situ pore water pressures and ground motions during the 1987 Chiba-Toho-Oki earthquake', *Soils and Foundations*, **29**, No. 4, 75-90 (1989).
2. Iwasaki, Y., and Tai, M., 'Strong motion records at Kobe Port Island', *Soils and Foundations*, Special Issue: Kobe, 29-40 (1996).
3. Zeghal, M. and Elgamal, A.-W., 'Analysis of site liquefaction using earthquake records', *Jour. Geotech. Engrg.*, ASCE, **120**, 996-1017 (1994).
4. Elgamal, A.-W., Zeghal, M., Tang, H.T., and Stepp, J.C., 'Lotung Downhole Seismic Array. I: Evaluation of Site Dynamic Properties', *Jour. Geotech. Engrg.*, ASCE, **121**, 350-362 (1994).
5. Zeghal, M., Elgamal, A.-W., Tang, H.T. and Stepp, J.C., 'Lotung Downhole Array. II: Evaluation of Soil Nonlinear Properties', *Jour. Geotech. Engrg.*, ASCE, **121**, 363-378 (1994).
6. Chang, C.-Y., Mok, C.M., Power, M.S., Tang, Y.K., Tang, H.T. and Stepp, J.C., 'Development of shear modulus reduction curves based on Lotung ground motion data', *Proc. 2nd Int. Conf. Recent Adv. Geotech. Earthq. Engrg. Soil Dyns.*, St Louis, 111-118 (1991).
7. Wen, K.-L., Beresnev, I.A. and Yeh, Y.T., 'Investigation of non-linear site amplification at two downhole strong ground motion arrays in Taiwan', *Earthq. Engrg. Struct. Dyns.*, **24**, 313-324 (1995).
8. Li, X.S., Shen, C.K. and Wang, Z.L., 'Fully coupled site response analysis for 1986 Lotung earthquake', *Jour. Geotech. Engrg.*, ASCE, **124**, 560-573 (1998).
9. Kazama, M., 'Nonlinear dynamic behavior of the ground inferred from strong motion array records at Kobe Port Island during the 1995 Hyogo-Ken Nanbu earthquake', *Proc. Int. Workshop on Site Response*, Yokosuka, Japan, **2**, 185-199 (1996).
10. Seed, H.B. and Idriss, I.M., 'Soil moduli and damping factors for dynamic response analyses', Earthquake Engineering Research Report EERC 70-10, University of California, Berkeley, 1970.
11. Bendat, J.S. and Piersol, A.G., *Engineering Application of Correlation and Spectral Analysis*, Wiley, New York, 1980.
12. Elgamal, A.-W., Zeghal, M., and Parra, E., 'Liquefaction of reclaimed land in Kobe, Japan', *Jour. Geotech. Engrg.*, ASCE, **122**, No. 1, 39-49 (1996).



13. Press, W.H., Flannery, B.P., Teukolsky, S.A., and Vetterling, W.T., *Numerical Recipes. The art of scientific computing*, Cambridge Press, New York, 1988.
14. Youd, T.L. and Holtzer, T.L. "Piezometer performance at Wildlife Liquefaction Site, California." *Jour. Geotech. Engg.*, ASCE, **120**, pp.975-995 (1994).
15. Holzer, T.L., Youd, T.L., and Hanks, T.C. "Dynamics of liquefaction during the Superstition Hills, California, Earthquake." *Science*, **244**, April 7, 56-59 (1989).
16. Archuleta, R.J. "Direct observation of nonlinearity in accelerograms." *Proc. 2nd Int. Symp. Effects of Surface Geology on Seismic Motion*, eds. K. Irikura, K. Kudo, H. Okada and T. Sasatani, A.A Balkema, pp.787-792 (1998).



APPENDIX A

ACCURACY OF SHEAR WAVE VELOCITY ESTIMATES

There are well defined limits on the accuracy of any estimated shear wave velocity based on downhole acceleration measurements. The accuracy depends upon the size of the digitization time step for the acceleration record. We cannot hope to estimate the travel time between two instruments to an accuracy smaller than the digitization time step. This is made clear from the definition of the discrete time series correlation shown in equation (1). In that equation the indices k and m identify discrete readings within the acceleration records. Changing m by one unit will move the correlation Γ by one digitised time step. Thus the greatest value of Γ (used to identify the lag time) has a resolution of one time step. We can expect the accuracy of the time lag to therefore be plus or minus one-half the digitization time step.

Let Δt denote the digitization time step associated with a set of downhole records and let h represent the separation distance between two instruments, say A and B . Suppose the estimated travel time between A and B at some point during the earthquake is T_{AB} . T_{AB} may be determined using the time compression method or from any other method for interpreting the records such as the use of individual window correlations. The estimated *nominal* shear wave velocity at that point during the earthquake is given by

$$\tilde{c} = \frac{h}{T_{AB}} \quad (a1)$$

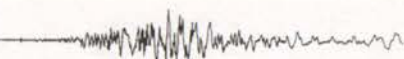
But we note that the limit of resolution on T_{AB} is $\pm \frac{1}{2} \Delta t$. Thus equation (a1) should be replaced by

$$c = \frac{h}{T_{AB} \pm \Delta t/2} = \frac{h}{T_{AB}} \left(\frac{1}{1 \pm \Delta t/2T_{AB}} \right) \quad (a2)$$

Where c is the actual estimate for the wave speed. We can expand the term in brackets in equation (a2) as a Taylor series.

$$c = \frac{h}{T_{AB}} \left(1 \mp \frac{\Delta t}{2T_{AB}} + \left(\frac{\Delta t}{2T_{AB}} \right)^2 \mp \left(\frac{\Delta t}{2T_{AB}} \right)^3 + \dots \right) \quad (a3)$$

Truncating the series and using the *nominal* wave speed defined in equation (a1) gives



$$c = \tilde{c} \mp \frac{\tilde{c} \Delta t}{2T_{AB}} = \tilde{c} \mp \frac{\tilde{c}^2 \Delta t}{2h} \quad (a4)$$

So we find the limits of accuracy for any estimate for shear wave velocity based on downhole measurements are $\pm \tilde{c}^2 \Delta t / 2h$.

If the nominal wave speed \tilde{c} is small, for example after significant amounts of softening have occurred, then the accuracy will generally be reasonably good. The accuracy decreases rapidly when \tilde{c} takes on greater values. This aspect is made clear in the East-West Kobe Port Island data where the small time stretching at 12 seconds led to the apparent sharp increase in shear wave velocity seen in Figure 17. The estimated wave speed increased from roughly 210 m/s to nearly 300 m/s, before dropping radically.

Figure A1 shows a graph of the magnitude of the wave speed resolution $\tilde{c}^2 \Delta t / 2h$ plotted versus the instrument separation h for a range of nominal wave velocities \tilde{c} and Δt equal to 0.01 seconds. Evidently significant errors are always possible whenever the nominal wave speed is large. The accuracy is improved by greater instrument spacing, but this is not an argument for placing instruments further apart. In fact closer instrument spacing is regarded as very desirable for other aspects of downhole record interpretation.

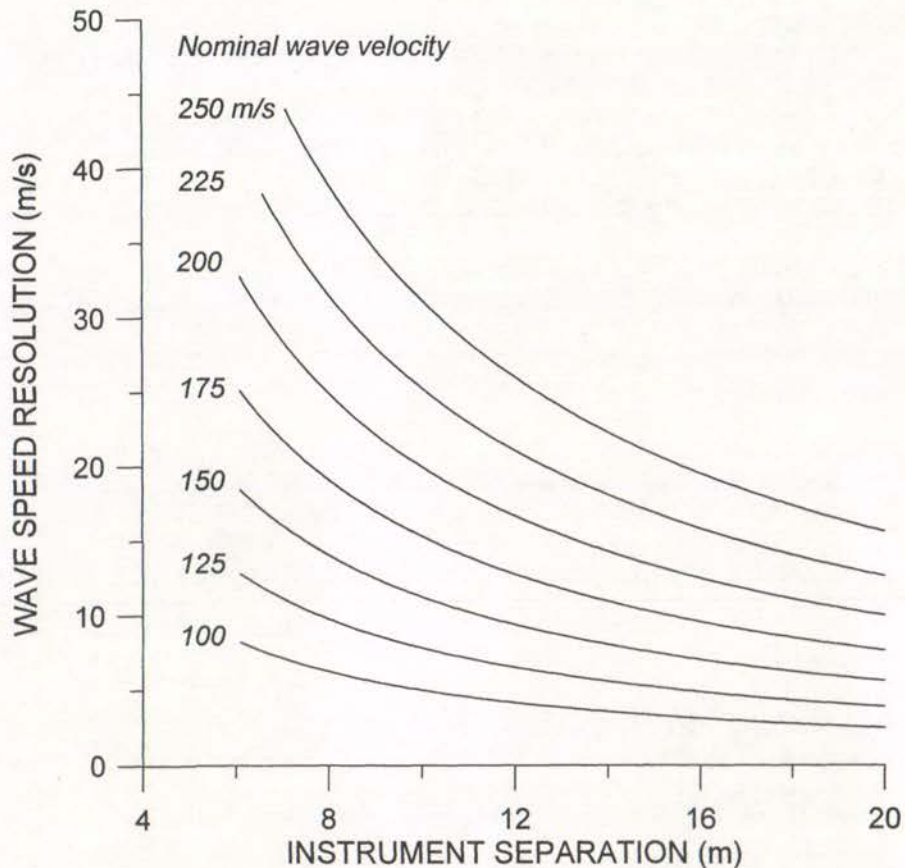
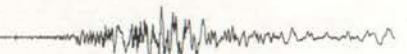


Figure A1. Estimated shear wave velocity resolution as a function of instrument separation for a selection of nominal velocity values



APPENDIX B

PROGRAM SMONE33

This appendix contains the FORTRAN listing for the program SMONE33, the main program used to generate the time compression results contained in this report. The listing contains several subprograms from reference 13. These are identified by the copyrights associated with each subprogram. In general the coding using upper case letters has been specifically written for the time compression algorithm. Coding written in lower case letters is from reference 13.

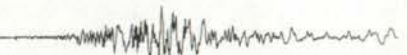
PROGRAM SMONE33

```
C  USES TIME COMPRESSION TO APPROXIMATE SHEAR MODULUS SOFTENING
C  BASED ON DOWNHOLE ACCELERATION RECORDS. THIS VERSION COMPRESSES
C  ONE TIME INCREMENT AT A TIME. OPTIMISATION IS BY GOLDEN SECTION.
C  OUTPUT IS ON KORREL2.DAT.
C
C  ADDITIONAL OUTPUT IN THIS VERSION IS THE TIME COMPRESSED DATA
C  ON FILE TCOMP.DAT. FOUR VECTORS ARE WRITTEN: TIME, DATA0,
C  DATA1 AND DATA2. DATA0 IS THE UNCOMPRESSED UPPER ACCELERATIONS.
C  DATA1 IS THE TIME COMPRESSED UPPER DATA. DATA2 IS THE UNCHANGED
C  LOWER DATA RECORD.
C
C  CONSTANTS:
C  NTOT = NUMBER OF DATA POINTS IN ACCELERATION TIME HISTORY
C  ITER = NUMBER OF ITERATIONS USED
C  NWIN = SIZE OF WINDOW FOR PEAK CORRELATION SEARCH
C  FTOL = MINIMUM TOLERANCE FOR DONENESS
C  DT = TIME STEP FOR ACCELERATION TIME HISTORY
C  DELTA0 = INITIAL INCREMENT OF TIME COMPRESSION
C
C  THE FUNCTION KORREL CARRIES OUT THE CROSS CORRELATION OF THE
C  TWO RECORDS AND THEN SEARCHES FOR THE PEAK VALUE. IT RETURNS
C  THAT VALUE (AS KORREL ITSELF) AS WELL AS THE ASSOCIATED TIME
C  LAG AS THE INTEGER MLAG. NOTE THAT THE DATA FILES DATA(N), DATA0(N)
C  DATA1(N) AND DATA2(N) MUST HAVE LENGTHS THAT ARE MULTIPLES OF 2.
C
C  THE VECTOR TSTRT CONTAINS THE TIME INTERVALS FOR WHICH
C  COMPRESSION IS CARRIED OUT. IN EACH TIME INCREMENT THE AMOUNT
C  OF COMPRESSION (PDELTA) IS ADJUSTED TO MAXIMISE THE CORRELATION.
C
C  OPTIMISATION OF THE CORRELATION IS DONE WITH SUBROUTINE MNBRAK
C  AND FUNCTION GOLDEN.
C
INTEGER NTOT,N2,NP,MP
REAL KORREL
COMMON/CON/ NTOT, TG(2), DT, K1,
$ K2, NP, MP, NWIN,
$ MLAG, CNORM
COMMON/CORL/ T(16384), data(16384), data1(16384), data2(16384),
$ ans(32768)
REAL acc(16), P(3), Y(3),
$ DATA0(16384), TSTRT(500)
DATA SMALL/1.E-3/, delta0/0.002/
```

```

C
OPEN(3,FILE='TDAT3.DAT',STATUS='OLD')
KC1=1
KC2=2
C
C READ THE DATA
C
N=0
11 READ(3,*,END=12)TT,acc
N=N+1
T(N)=TT
DATA1(N)=acc(KC1)
DATA2(N)=acc(KC2)
DATA(N)=acc(KC1)
DATA0(N)=acc(KC1)
GO TO 11
12 WRITE(6,*)N,' DATA POINTS DETECTED'
NTOT=N
N2=2*NTOT
CLOSE(3)
CN1=0.0
CN2=0.0
DO 15 N=1,NTOT
CN1=CN1+DATA1(N)*DATA1(N)
CN2=CN2+DATA2(N)*DATA2(N)
15 CONTINUE
CNORM=SQRT(CN1)*SQRT(CN2)
C
C READ THE PARAMETER FILE
C
WRITE(6,*)
OPEN(4,FILE='SMOD.DAT',STATUS='OLD')
READ(4,*)DT,FTOL,NWIN,ITMAX
CLOSE(4)
NP=1
MP=2
WRITE(6,*)
WRITE(6,*)'INPUT PARAMETERS: DT FTOL NWIN'
WRITE(6,23)DT,FTOL,NWIN
C
C FIND THE INITIAL PEAK CORRELATION
C
call correl(data1,data2,NTOT,ans)
FCORR=ANS(1)
DO 16 M=1,NWIN-1
IF(ANS(M+1).LT.FCORR)GO TO 16
FCORR=ANS(M+1)
MLAG=M+1
16 CONTINUE
FCORR=FCORR/CNORM
WRITE(6,*)'THE INITIAL VALUE OF FCORR IS: ',FCORR,' AT M =',MLAG
C
23 FORMAT(14X,F10.4,e12.4,I7)
WRITE(6,*)
c WRITE(6,*)'ENTER INITIAL TIME STEP '
c READ(5,*)DELTA0
c WRITE(6,*)
C
OPEN(2,FILE='KORREL2.DAT',STATUS='NEW')
PDELSUM=0.0

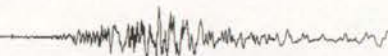
```



```

C
C BEGIN COMPRESSION
C
CALL SOFT(KSOFT,TSTRT)
WRITE(6,*)'
WRITE(6,*) CYCLE   TSTRT   PDELTA   PDELSUM
& YMAX   MLAG'
KS=1
KSOFT=KSOFT-1
35 IF(KS.GE.KSOFT)GO TO 128
TG(1)=TSTRT(KS)
TG(2)=TSTRT(KS+1)
FKTG=(TG(2)-TG(1))*10.
KTG=FKTG+SMALL
KS=KS+1
C
C SET INITIAL POINTS FOR OPTIMISATION
C
P(1)=-delta0
P(2)=DELTA0
test=korrel(P(1))
C
C BEGIN THE OPTIMISATION
C FIRST MNBRAK BRACKETS A MAXIMUM CORRELATION POINT
C THEN GOLDEN REFINES THE MAXIMUM TO THE REQUIRED TOLERANCE
C RESULTS ARE: PDELTA = LAG TIME FOR OPTIMAL COMPRESSION
C           YMAX = CORRELATION FOR PDELTA
C
CALL MNBRAK(P(1),P(2),P(3),Y(1),Y(2),Y(3),KORREL)
YMAX=-GOLDEN(P(1),P(2),P(3),KORREL,FTOL,PDELTA)
C
WRITE(6,110)KS,TSTRT(KS),-PDELTA,-PDELSUM,YMAX,MLAG
DO 75 JTG=1,KTG
TW=TG(1)+FLOAT(JTG)*0.1
PDELSUM=PDELSUM+PDELTA/FLOAT(KTG)
WRITE(2,111)TW,-PDELTA,-PDELSUM,YMAX
75 CONTINUE
110 FORMAT(I7,F15.5,2E15.5,F15.5,I6)
111 FORMAT(5E18.8)
C
C HERE RESET THE TIME BASE
C
CALL STRCH(PDELTA)
DO 118 N=1,NTOT
DATA(N)=DATA1(N)
118 CONTINUE
GO TO 35
C
128 CONTINUE
OPEN(9,FILE='TCOMP.DAT',STATUS='NEW')
DO 155 N=1,NTOT
WRITE(9,111)T(N),DATA0(N),DATA1(N),DATA2(N)
155 CONTINUE
C
call correl(data1,data2,NTOT,ans)
FCORR=ANS(1)
DO 232 M=1,NWIN-1
IF(ANS(M+1).LT.FCORR)GO TO 232
FCORR=ANS(M+1)
MLAG=M+1

```



```

232 CONTINUE
FCORR=FCORR/CNORM
WRITE(6,*)'LAST VALUE OF YMAX WAS:',YMAX
WRITE(6,*)'THE VALUE OF FCORR IS: ',FCORR,' AT M =',MLAG
WRITE(6,*)
WRITE(6,*)'TO WRITE THE CORREL FILE ENTER 1'
READ(5,*)ICSW
IF(ICSW.EQ.1)CALL COR(DT,NTOT,NWIN,CNORM,ANS)
STOP
END
C
SUBROUTINE COR(DT,NTOT,NWIN,CNORM,ANS)
DIMENSION ANS(32768), CORR(1000), TW(1000)
OPEN(8,FILE='CORREL.DAT',STATUS='NEW')
KNT=0
TW(1)=-NWIN*DT
DO 20 K=2,(2*NWIN)
20 TW(K)=TW(K-1)+DT
DO 31 M=(NTOT-NWIN),NTOT-1
KNT=KNT+1
31 CORR(KNT)=ANS(M)/CNORM
DO 32 M=1,NWIN
KNT=KNT+1
32 CORR(KNT)=ANS(M)/CNORM
DO 41 KNT=1,(2*NWIN)
41 WRITE(8,44)TW(KNT),CORR(KNT)
44 FORMAT(2F15.5)
RETURN
END
C
REAL FUNCTION KORREL(PDELTA)
COMMON/CON/ NTOT, TG(2), DT, K1,
$ K2, NP, MP, NWIN,
$ MLAG, CNORM
COMMON/CORL/ T(16384), data(16384), data1(16384), data2(16384),
$ ans(32768)
C
CALL STRCH(PDELTA)
C
call correl(data1,data2,NTOT,ans)
C
KORREL=ANS(1)
DO 32 M=1,NWIN-1
IF(ANS(M+1).LT.KORREL)GO TO 32
KORREL=ANS(M+1)
MLAG=M+1
32 CONTINUE
KORREL=-KORREL/CNORM
RETURN
END
C
C
SUBROUTINE STRCH(PDELTA)
C HERE TIME IS COMPRESSED IN THE ARRAY DATA
C
COMMON/CON/ NTOT, TG(2), DT, K1,
$ K2, NP, MP, NWIN,
$ MLAG, CNORM
COMMON/CORL/ T(16384), data(16384), data1(16384), data2(16384),
$ ans(32768)

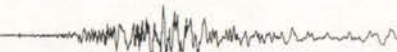
```



```

DIMENSION N1(2), TTMP(16384), DTMP(16384)
C
DO 5 M=1,MP
5 N1(M)=TG(M)/DT
DO 11 J=1,NTOT
11 DTMP(J)=DATA(J)
C
C BEGIN STRETCHING AT N1
C
DO 31 J=1,N1(1)
31 TTMP(J)=T(J)
C
I1=N1(1)+1
I2=N1(2)
DO 32 J=I1,I2
32 TTMP(J)=T(J)
$ +PDELTA*(T(J)-TG(1))/(TG(2)-TG(1))
C
DO 34 J=I2,NTOT
34 TTMP(J)=T(J)+PDELTA
C
C INTERPOLATE NEW DATA1 VECTOR
C
JJ=N1(1)
JK=JJ+1
TP1=TTMP(JJ)
TP2=TTMP(JK)
DO 51 J=JK,NTOT
TT=T(J)
44 IF(TT.LT.TP2)GO TO 50
JJ=JJ+1
IF(JJ.GT.NTOT)GO TO 61
TP1=TP2
TP2=TTMP(JJ+1)
GO TO 44
50 DATA1(J)=DTMP(JJ)+(DTMP(JJ+1)-DTMP(JJ))*(TT-TP1)/(TP2-TP1)
51 CONTINUE
61 CONTINUE
JA=J
DO 65 J=JA,NTOT
65 DATA1(J)=0.0
RETURN
END
C
C
SUBROUTINE correl(data1,data2,n,ans)
INTEGER n,NMAX
REAL data1(n),data2(n)
COMPLEX ans(n)
PARAMETER (NMAX=16384)
CU USES realft,twofft
INTEGER i,no2
COMPLEX fft(NMAX)
call twofft(data1,data2,fft,ans,n)
no2=n/2
do 11 i=1,no2+1
ans(i)=fft(i)*conjg(ans(i))/float(no2)
11 continue
ans(1)=cmlpx(real(ans(1)),real(ans(no2+1)))
call realft(ans,n,-1)

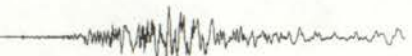
```



```

return
END
C (C) Copr. 1986-92 Numerical Recipes Software 21"$!6W.
SUBROUTINE twofit(data1,data2,fft1,fft2,n)
INTEGER n
REAL data1(n),data2(n)
COMPLEX fft1(n),fft2(n)
CU USES four1
INTEGER j,n2
COMPLEX h1,h2,c1,c2
c1=cmplx(0.5,0.0)
c2=cmplx(0.0,-0.5)
do 11 j=1,n
fft1(j)=cmplx(data1(j),data2(j))
11 continue
call four1(fft1,n,1)
fft2(1)=cmplx(aimag(fft1(1)),0.0)
fft1(1)=cmplx(real(fft1(1)),0.0)
n2=n+2
do 12 j=2,n/2+1
h1=c1*(fft1(j)+conjg(fft1(n2-j)))
h2=c2*(fft1(j)-conjg(fft1(n2-j)))
fft1(j)=h1
fft1(n2-j)=conjg(h1)
fft2(j)=h2
fft2(n2-j)=conjg(h2)
12 continue
return
END
C
SUBROUTINE realft(data,n,isign)
INTEGER isign,n
REAL data(n)
CU USES four1
INTEGER i,i1,i2,i3,i4,n2p3
REAL c1,c2,h1i,h1r,h2i,h2r,wis,wrs
DOUBLE PRECISION theta,wi,wpi,wpr,wr,wtemp
theta=3.141592653589793d0/dble(n/2)
c1=0.5
if (isign.eq.1) then
c2=-0.5
call four1(data,n/2,+1)
else
c2=0.5
theta=-theta
endif
wpr=-2.0d0*sin(0.5d0*theta)**2
wpi=sin(theta)
wr=1.0d0+wpr
wi=wpi
n2p3=n+3
do 11 i=2,n/4
i1=2*i-1
i2=i1+1
i3=n2p3-i2
i4=i3+1
wrs=sngl(wr)
wis=sngl(wi)
h1r=c1*(data(i1)+data(i3))
h1i=c1*(data(i2)-data(i4))

```



```

h2r=-c2*(data(i2)+data(i4))
h2i=c2*(data(i1)-data(i3))
data(i1)=h1r+wrs*h2r-wis*h2i
data(i2)=h1i+wrs*h2i+wis*h2r
data(i3)=h1r-wrs*h2r+wis*h2i
data(i4)=-h1i+wrs*h2i+wis*h2r
wtemp=wr
wr=wr*wpr-wi*wpi+wr
wi=wi*wpr+wtemp*wpi+wi
11 continue
if (isign.eq.1) then
h1r=data(1)
data(1)=h1r+data(2)
data(2)=h1r-data(2)
else
h1r=data(1)
data(1)=c1*(h1r+data(2))
data(2)=c1*(h1r-data(2))
call four1(data,n/2,-1)
endif
return
END
C (C) Copr. 1986-92 Numerical Recipes Software 21"$!6W.
SUBROUTINE four1(data,nn,isign)
INTEGER isign,nn
REAL data(2*nn)
INTEGER i,istep,j,m,mmax,n
REAL tempi,tempr
DOUBLE PRECISION theta,wi,wpi,wpr,wr,wtemp
n=2*nn
j=1
do 11 i=1,n,2
if(j.gt.i)then
tempr=data(j)
tempi=data(j+1)
data(j)=data(i)
data(j+1)=data(i+1)
data(i)=tempr
data(i+1)=tempi
endif
m=n/2
1 if ((m.ge.2).and.(j.gt.m)) then
j=j-m
m=m/2
goto 1
endif
j=j+m
11 continue
mmax=2
2 if (n.gt.mmax) then
istep=2*mmax
theta=6.28318530717959d0/(isign*mmax)
wpr=-2.d0*sin(0.5d0*theta)**2
wpi=sin(theta)
wr=1.d0
wi=0.d0
do 13 m=1,mmax,2
do 12 i=m,n,istep
j=i+mmax
tempr=sngl(wr)*data(j)-sngl(wi)*data(j+1)

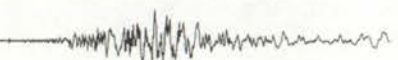
```



```

    tempi=sngl(wr)*data(j+1)+sngl(wi)*data(j)
    data(j)=data(i)-tempr
    data(j+1)=data(i+1)-tempi
    data(i)=data(i)+tempr
    data(i+1)=data(i+1)+tempi
12  continue
    wtemp=wr
    wr=wr*wpr-wi*wpi+wr
    wi=wi*wpr+wtemp*wpi+wi
13  continue
    mmax=istep
    goto 2
    endif
    return
    END
C
SUBROUTINE mnbrak(ax,bx,cx,fa,fb,fc,KORREL)
REAL ax,bx,cx,fa,fb,fc,KORREL,GOLD,GLIMIT,TINY
EXTERNAL KORREL
PARAMETER (GOLD=1.618034, GLIMIT=100., TINY=1.e-20)
REAL dum,fu,q,r,u,ulim
fa=KORREL(ax)
fb=KORREL(bx)
if(fb.gt.fa)then
    dum=ax
    ax=bx
    bx=dum
    dum=fb
    fb=fa
    fa=dum
endif
cx=bx+GOLD*(bx-ax)
fc=KORREL(cx)
1  if(fb.ge.fc)then
    r=(bx-ax)*(fb-fc)
    q=(bx-cx)*(fb-fa)
    u=bx-((bx-cx)*q-(bx-ax)*r)/(2.*sign(max(abs(q-r),TINY),q-r))
    ulim=bx+GLIMIT*(cx-bx)
    if((bx-u)*(u-cx).gt.0.)then
        fu=KORREL(u)
        if(fu.lt.fc)then
            ax=bx
            fa=fb
            bx=u
            fb=fu
            return
        else if(fu.gt.fb)then
            cx=u
            fc=fu
            return
        endif
        u=cx+GOLD*(cx-bx)
        fu=KORREL(u)
    else if((cx-u)*(u-ulim).gt.0.)then
        fu=KORREL(u)
        if(fu.lt.fc)then
            bx=cx
            cx=u
            u=cx+GOLD*(cx-bx)
            fb=fc

```



```

    fc=fu
    fu=KORREL(u)
  endif
else if((u-ulim)*(ulim-cx).ge.0.)then
  u=ulim
  fu=KORREL(u)
else
  u=cx+GOLD*(cx-bx)
  fu=KORREL(u)
endif
ax=bx
bx=cx
cx=u
fa=fb
fb=fc
fc=fu
goto 1
endif
return
END
C (C) Copr. 1986-92 Numerical Recipes Software 21"$!6W.
FUNCTION golden(ax,bx,cx,KORREL,tol,xmin)
REAL golden,ax,bx,cx,tol,xmin,KORREL,R,C
EXTERNAL KORREL
PARAMETER (R=.61803399,C=1.-R)
REAL f1,f2,x0,x1,x2,x3
C   WRITE(6,*)'A1,A2,A3:',AX,BX,CX
x0=ax
x3=cx
if(abs(cx-bx).gt.abs(bx-ax))then
  x1=bx
  x2=bx+C*(cx-bx)
else
  x2=bx
  x1=bx-C*(bx-ax)
endif
C   WRITE(6,*)'X0-X3:',X0,X1,X2,X3
C   WRITE(6,*)'START LOOP '
f1=KORREL(x1)
f2=KORREL(x2)
1  if(abs(x3-x0).gt.tol*(abs(x1)+abs(x2)))then
    if(f2.lt.f1)then
      x0=x1
      x1=x2
      x2=R*x1+C*x3
      f1=f2
      f2=KORREL(x2)
    else
      x3=x2
      x2=x1
      x1=R*x2+C*x0
      f2=f1
      f1=KORREL(x1)
    endif
C   WRITE(6,*)'X0-X3:',X0,X1,X2,X3
C   PAUSE
goto 1
endif
if(f1.lt.f2)then
  golden=f1

```



```
xmin=x1
else
golden=f2
xmin=x2
endif
return
END
```

C (C) Copr. 1986-92 Numerical Recipes Software 21"\$!6W.

```
C
SUBROUTINE SOFT(KSOFT,TSTRT)
DIMENSION TSTRT(500)
WRITE(6,*)'ENTER START AND STOP TIMES'
READ(5,*)T0,TF
WRITE(6,*)'ENTER TIME INCREMENT'
READ(5,*)DT
```

```
C
T=T0-DT
KSOFT=1
10 T=T+DT
IF(T.GT.TF)RETURN
TSTRT(KSOFT)=T
KSOFT=KSOFT+1
GO TO 10
END
```

